APL Materials

Inkjet printing for flexible and wearable electronics

Cite as: APL Mater. **8**, 120705 (2020); https://doi.org/10.1063/5.0031669
Submitted: 02 October 2020 • Accepted: 25 November 2020 • Published Online: 16 December 2020

Ke Yan, Jiean Li, Lijia Pan, et al.

Inkjet printing for flexible and wearable electronics

Cite as: APL Mater. 8, 120705 (2020); doi: 10.1063/5.0031669
Submitted: 2 October 2020 • Accepted: 25 November 2020 •
Published Online: 16 December 2020

Ke Yan, Jiean Li, Lijia Pan,[a] and Yi Shi

AFFILIATIONS

Collaborative Innovation Center of Advanced Microstructures, Jiangsu Provincial Key Laboratory of Photonic and Electronic Materials, School of Electronic Science and Engineering, Nanjing University, Nanjing 210093, China

[a]Author to whom correspondence should be addressed: ljpan@nju.edu.cn

ABSTRACT

Flexible and wearable electronic devices are emerging as the novel platform for portable health monitoring, human–machine interaction, and some other electronic/optic applications. Future development of human-friendly smart electronics relies on efficient manufacturing and processing of advanced functional materials on flexible/stretchable substrates with effective device integration. Inkjet printing, known as a highly efficient solution-based printing and patterning technology with low-cost, high-quality, and high-throughput advantages, suits large-scale fabrication of flexible and wearable electronics. Over the years, researchers focused on high pattern resolution and uniformity on flexible substrates for advanced electrical/optical performances by various inkjet printing techniques. Different ink materials that can realize multiple functions have been fully investigated for achieving favorable printability and desired interactions with the substrates. Here, the most recently reported inkjet printing strategies, functional ink materials, and diverse inkjet-printed wearable electronic devices for practical applications (e.g., sensors, displays, transistors, and energy storage devices) are summarized. An outlook on future challenges as well as opportunities of inkjet-printed flexible and wearable electronics for research development and industrial commercialization is also presented.

I. INTRODUCTION

The past few years have witnessed boost in the research of flexible and wearable electronics on skin surfaces or integrated into cloth for versatile functions concerning healthcare monitoring, signal sensing and analyzing, information displaying, and human–machine interaction.[1–4] Preliminary wearable electronic devices such as the iWatch have been playing increasingly significant roles in people's daily lives. However, most of the current wearable devices are made of traditional electronic components and circuits on rigid substrates, which severely limit the device's functionality and wearing comfort. Future development of flexible and wearable electronics relies on efficient manufacturing and processing on flexible/stretchable substrates in a strain-accommodating architecture to meet the demands of "real" wearable applications.[5–7] Fabrication of flexible and wearable electronics with flexibility/stretchability is facing a variety of obstacles, specifically the layout of electronic components and circuits, stretchable circuit deposition with high electrical conductivity, and flexible integration of functional components and energy supplies, together with the platform in realizing practical manufacturing.[8–10] Owing to the superiority in low-cost and simple manufacturing, printing techniques such as flexography, rotogravure, screen printing, roll-to-roll printing, and inkjet printing are specially developed for continuous processing of functional material patterning on flexible substrates and devices.[11–13]

In recent years, the dramatic growth of research interest has focused on inkjet printing, which is a mask-free printing technology and realizes non-contact patterning on various substrates by programming the motion of the printing nozzle.[14] The operation modes of inkjet printing are (i) drop-on-demand (DoD) printing, which delivers droplets induced by thermal bubbles or a piezoelectric actuator, and (ii) continuous inkjet (CIJ) printing, which generates a continuous ink stream through a nozzle by the electrostatic or magnetic field. Inkjet printing has various intrinsic merits, such as high manufacturing throughput, large-scale patterning, good

biocompatibility, and accurate deposition on unlimited substrates, which are desired for advanced flexible and wearable electronics fabrication. High patterning resolution of sub-100 nm can be realized for more sophisticated electronics over other solution processes, such as dip-coating, spin-coating, drop-casting, and spraying.[15,16] Moreover, the drop-on-demand concept drastically reduces the consumption of costly ink materials owing to the micro-droplet deposition and programmable patterning. However, there still exist many challenges that make this technology relatively unfavorable at this stage. These challenges include, but are not limited to, the prevention of nozzle clogging, restraint of the coffee-ring effect, enhancement of ink dispersibility, reduction of sintering temperature for flexible substrates, promotion of electrical and mechanical properties, and device designing for human body integration.

Here, we review the fundamental issues as well as recent progress in inkjet printing technology and elucidate the most advanced flexible and wearable electronics by inkjet printing. First, the ink's printability and interaction with substrates are discussed for comprehension of the pattern's resolution and uniformity. Then, improvement in flexibility, stretchability, and durability on flexible substrates such as polymers, papers, and textiles are demonstrated. Moreover, we summarize various ink materials for inkjet printing (e.g., polymer, metal, carbon, and, in particular, the surging hydrogels and 2D materials), which offer novel specialties for high-performance electronic devices, and discuss some novel strategies that overcome the potential limitations of scalable production in inkjet printing. Finally, we provide some recently reported cases of advanced inkjet-printed flexible and wearable electronics with state-of-the-art performances for applications such as sensors, displays, transistors, energy storage devices, and some other electronics.

II. INKJET PRINTING STRATEGIES

Fabrication of flexible and wearable electronics using inkjet printing technology faces a series of challenges concerning pattern resolution, electrical conductivity, device stretchability, and mechanical durability in practical applications. The detailed strategies for improving the quality of inkjet printing and effective design for flexible and wearable applications are discussed below.

A. Ink's property

The property of ink has been an important research subject for printability, which is determined by the ink materials and the solvent. The ejection of a well-formed single drop without any separated tail (i.e., satellite droplets) represents a good printability. The physical and rheological properties of the liquid ink can be characterized by the dimensionless numbers such as the Reynolds number (R_e), Weber number (W_e), and the Ohnesorge number (Oh),

$$R_e = \frac{v\rho d}{\eta},$$

$$W_e = \frac{v^2\rho a}{\gamma},$$

$$Oh = \frac{\sqrt{W_e}}{R_e} = \frac{\eta}{\sqrt{\gamma\rho d}},$$

where v, ρ, η, γ, and d refer to the velocity, density, dynamic viscosity, surface tension, and characteristic length, respectively. For an ink drop ejected by a printer, the characteristic length relates to the diameter of the nozzle, while the parameter Z (=1/Oh) indicates the printability of the ink drop. To print a stable droplet, $1 < Z < 10$ are widely accepted as the optimum range according to numerical computations. The effects of viscous dissipation and capillary force would prevent drop ejection when $Z < 1$, whereas inks with $Z > 10$ would form primary drops with unstable satellite droplets. Some experimental studies showed the variation of the boundary value of Z for successful drop-on-demand inkjet printing.[17,18] Liu and Derby demonstrated that the practical range for ink printability is bounded by both W_e ($2 < W_e < 25$) and Z ($2 < Z < 20$) for satellite-free drop-generation.[19] With the aid of laser-induced shockwaves, Delrot *et al.* extended the range of $0.67 < Z < 100$ by the flow-focusing effect and broke the limitations concerning the ink rheological properties and loading particle sizes.[20] The minimum velocity (v_{min}) for the droplet to break the fluid/air surface tension barrier at the nozzle is given by

$$v_{min} = \left(\frac{4\gamma}{\rho d_n}\right)^{\frac{1}{2}},$$

where d_n denotes the diameter of the printing nozzle. The typical nozzle of piezoelectric inkjet printing has a diameter of 10 μm–150 μm, which specifically depends on the ink properties and the applications. To achieve high-resolution printing, the nozzle inner size can be reduced for lowering the droplet volume (e.g., 20 μm to form the sub-1 pL droplet), but the diameter of the ink droplet is typically larger than that of the nozzle. For optimization of the printing resolution, the rheology of the ink and the functional particle sizes can be further controlled. The ink properties such as surface tension and density can be changed by altering the solvent, adding surfactants, adjusting the solute concentration, containing additives or binders, etc. Besides, the clogging of the nozzle challenges the continuous ejection especially of solid particles or in high-temperature processes.[21] To prevent nozzle clogging and form consistent droplets, the strategies of impurity filtration, viscosity reduction, and sufficiently low solvent volatility ought to be preliminarily considered. To avoid agglomeration of dispersed particles, the ink materials can be modified with functional groups (with hydrophobicity or hydrophilicity depending on the solvent) by introducing stabilizing agents (surfactants and polymers).[14,22] Most of the inks for inkjet printing behave in a linear Newtonian manner with a constant low viscosity over variable driving forces and shear rates, but non-Newtonian inks such as some viscoelastic polymer solutions also need to be investigated.[23]

B. Ink's interaction with the substrate

After being ejected from the nozzle, the well-formed ink droplets fly directly onto the targeted substrate and then spread before a liquid–solid phase change. Several physical forces, such as inertial forces, capillary forces, and gravitational forces, drive the impact process of a liquid drop onto the substrate.[24] High-speed camera systems can be used to capture the movement and behavior of instantaneously formed ink droplets. The impact of a

drop onto dry solid surfaces includes the impact-driven spreading, recoil-oscillation, and capillary-driven spreading.[25,26] In the entire process, the printed track or footprint diameter d_f is determined by the equilibrium contact angle on the substrate θ_{eqm} and the diameter of the droplet in air d_0 (d_f is linear with d_0 at a constant equilibrium contact angle) using the following equation:[24]

$$d_f = d_0 \sqrt[3]{\frac{8}{\tan\frac{\theta_{eqm}}{2}\cdot\left(3+\tan^2\frac{\theta_{eqm}}{2}\right)}}.$$

The printed dot dimension after the solvent evaporation is highly relevant to d_f. Therefore, the contact angle, which is under the function of the surface tension between solid, liquid, and air, also determined the pattern sizes. Generally, the interaction between ink and substrate is controlled by (i) changing the surface tension of the liquid ink with surfactants or bi-solvent, (ii) modifying the morphology and surface tension of the substrate, (iii) adjusting the drying atmospheres, and (iv) adopting a pre-patterned structure on the substrate.

C. High pattern resolution and uniformity

The high pattern resolution in inkjet printing is fundamental to the layout design of miniaturized devices integrating with the human body. The interactions of the ink droplet with the substrate, the solvent evaporation rate, and the capillary flow from the center to the periphery work together to determine the printed pattern's resolution and uniformity [Fig. 1(a)].[27] For the printed pattern's size confinement, the omniphobic fluoroalkylated modification of flexible paper (R^F paper) was proposed by Whitesides's group to increase the lateral resolution of the conductive pattern by inkjet printing [Fig. 1(b)].[28] The substrate with high surface energy was demonstrated to decrease the spreading degree and pattern size through decreasing static contact angle. Moreover, the three-phase contact line (TCL) of the printed droplet also influences the final printed pattern. Kuang *et al.* fabricated a low-adhesive substrate to help TCL slide inward in the drying process and spontaneously form a centralized deposition of ink nanoparticles (NPs) [Fig. 1(c)].[29] Wu *et al.* used a similar method and built the desired 3D morphology of inkjet-printed NPs by manipulating the TCL pinned on the hydrophilic patterns and de-wetted on the hydrophobic points.[30]

1. Coffee-ring effect

When the TCL of a drop is pinned during the evaporation, the solutes prefer accumulating and depositing along the drop periphery due to capillary flow, forming a ring-like morphology called the "coffee ring." To overcome the nonuniformity caused by the "coffee ring effect," many methods have been proposed including weakening the outward flow, increasing the inward Marangoni flow, and preventing the droplet pinning.[31,32] The surface-tension gradient induced by the solvent concentration or temperature difference can recirculate ink particles on the edge back to the center of the drop, which is called the Marangoni flow.[33,34] Hu *et al.* demonstrated a co-solvent binder-free black phosphorus (BP) ink with 10 vol. % alcohol in *N*-methylpyrrolidone (NMP), which inhibited the coffee-ring formation through the Marangoni flow.[35] This simple method showed a consistent (< 2% variation) and spatial-uniform (< 3.4% variation) inkjet-printed morphology for optoelectronics and photonics, especially the massive printing of quantum dot light-emitting diodes. Recently, self-assembly of NPs at the air–liquid interface was employed as an effective strategy to suppress the coffee-ring effect.[36] Al-Milaji *et al.* reported a novel "dual-droplet" inkjet printing that deposited a wetting droplet containing colloidal particles on a supporting droplet. The particles spread and self-assembled into a closely packed monolayer at the interface [Fig. 1(d)].[37] This "dual-droplet" inkjet printing configuration can produce a uniform deposition of NPs without limitation of materials or substrates. Liu *et al.* printed *in situ* crystallized perovskite-nanocomposite microarrays with additive polyvinylpyrrolidone (PVP), which eliminated the outward capillary flow by the spatial confinement of the perovskite/PVP nanocomposites to control microarray's morphology.[27] As for temperature-gradient induced Marangoni flow, most cases increased the deposition temperature to enhance the inward flow with elevated evaporation rate; rather, He *et al.* presented an ice-drying method for the suppression of the coffee-ring effect on various substrates [Fig. 1(e)].[38] By controlling the time delay and the ice-drying temperature, different inkjet-printed patterns (e.g., a uniform deposition, a central aggregation, and a "coffee eye") were obtained.

2. Nozzle diameter

Reducing the nozzle inner diameter is another obvious approach to decrease the drop size. However, it may have clogging problems and high hampering pressure at the nozzle tip that cause decreased mechanical durability and require extra driving forces to jet inks. Wu *et al.* proposed the liquid-repellent modification of the nozzle inner surface, and the modified omniphobic nozzle can print picoliter droplets of ink without extra driving forces.[39] Furthermore, the electric field induced Taylor cone can be employed to "pull" (rather than "push") the liquids from the nozzle, which is called electrohydrodynamic jet (e-jet or EHJ) printing.[40] The EHJ printing overcame ink-ejection difficulties in a small nozzle diameter of 30 nm[41] and achieved a sub-100 nm printing resolution with various applications.[42–44] Recently, EHJ printing was investigated to control the evolution of the "coffee ring" and improve the resolution of self-assembled Ag NP patterns with 3D morphology. A high pattern resolution of sub-50 nm linewidth could be realized via EHJ printing of 500 V by controlling the substrate wettability, the voltage duration, and the operation temperature [Fig. 1(f)].[45,46]

3. Ink spacing and interaction

The continuous patterns and printed lines require the isolated drops of inkjet printing to coalesce and overlap in high uniformity. Controlling drop spacing and coalescing time can prevent the formation of insulated drop beads or excessively wide lines.[47] Song's group reported utilizing the coffee-ring effect to print two parallel conducting metal lines with widths of 5 μm–10 μm in a single inkjet deposition process.[48] Moreover, it is also desired to fabricate 3D microstructures and patterning connections with overlapped droplets in the out-of-plane dimension by inkjet printing with the assistance of the electrical field, capillary force, and magnetic field. Onses *et al.* expanded this technology to fabricate hierarchical patterns of 3D block-copolymer films by combining inkjet printing with self-assembly.[43] It is still challenging to promote the 3D resolution of inkjet printing, but highly integrated functions of flexible

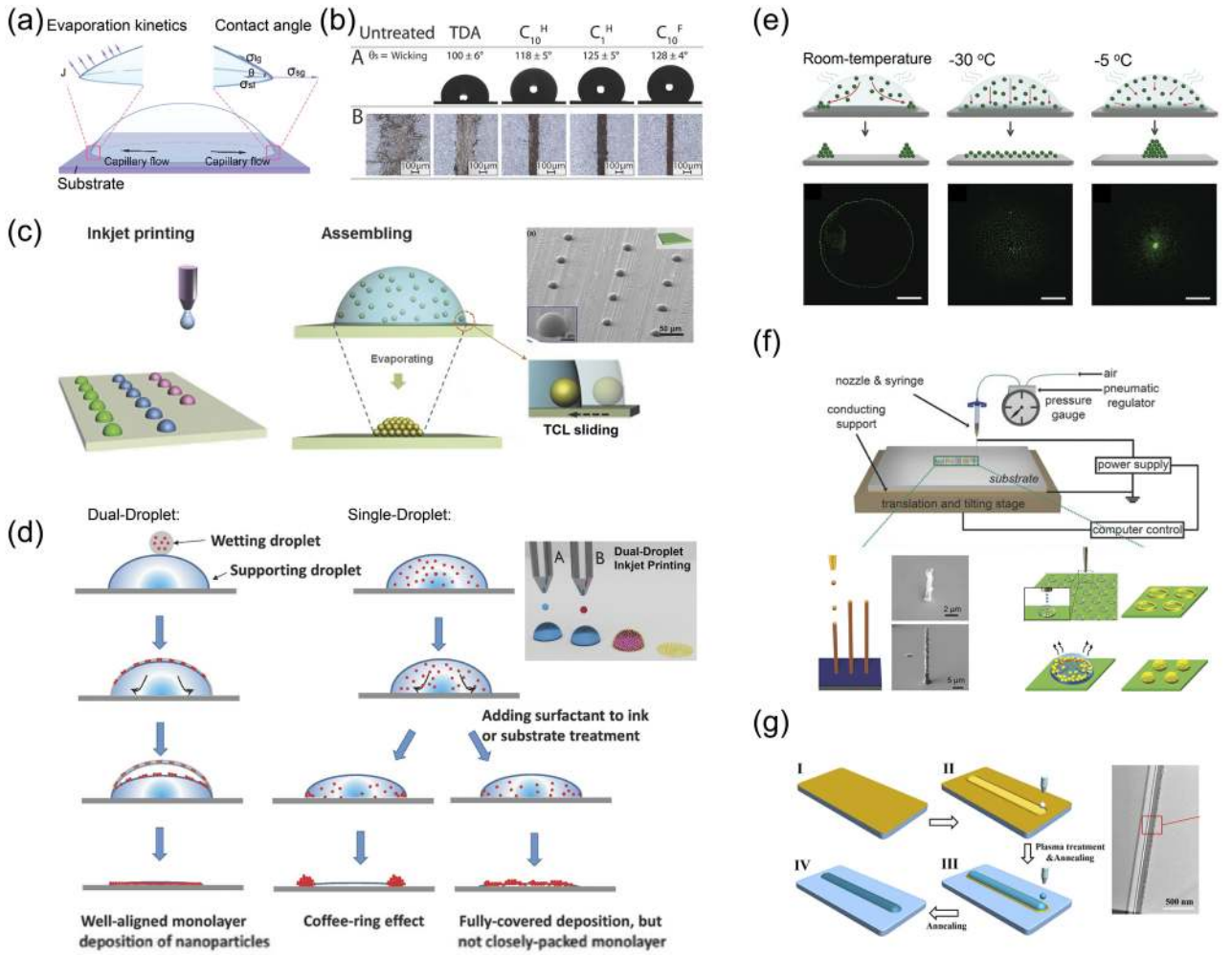

FIG. 1. (a) Schematic of solvent evaporation, capillary flow, and contact angle of the ink droplet.[27] Reproduced with permission from Liu *et al.*, ACS Nano **13**, 2042 (2019). Copyright 2019 American Chemical Society. (b) The printed pattern's resolution could be improved with the increased contact angle of ink droplets.[28] Reproduced with permission from Lessing *et al.*, Adv. Mater. **26**, 4677 (2014). Copyright 2014 Wiley-VCH. (c) Schematic of inkjet-printed centralized NPs on low-adhesive substrates with TCL sliding inward. Inset: the SEM image of the alignment of centralized NPs with high uniformity.[29] Reproduced with permission from Kuang *et al.*, Adv. Opt. Mater. **2**, 34 (2014). Copyright 2014 Wiley-VCH. (d) Schematic comparison of deposited patterns between "dual-droplet" inkjet printing and conventional inkjet printing. Inset: two nozzles were programmed to print supporting droplets and wetting droplets in sequence.[37] Reproduced with permission from Al-Milaji *et al.*, Adv. Mater. Interface **5**, 1701561 (2018). Copyright 2018 Wiley-VCH. (e) Ice-drying method for suppressing the coffee-ring effect and centralizing the deposition of ink NPs[38] (scale bar: 500 μm). Reproduced with permission from He *et al.*, Adv. Mater. Interface **6**, 1900446 (2019). Copyright 2019 Wiley-VCH. (f) EHJ printing controlling the growth of various 3D self-assembled patterns with high resolution.[45,46] Reproduced with permission from An *et al.*, Adv. Mater. **27**, 4322 (2015). Copyright 2015 Wiley-VCH. Reproduced with permission from Zhou *et al.*, Adv. Mater. Interfaces **6**, 1900912 (2019). Copyright 2019 Wiley-VCH. (g) Left: solvent etching and oxygen-plasma treatment for making surface-energy pre-patterns and (right) the cross-sectional STEM image of the printed high-resolution transistor.[57] Reproduced with permission from Zhou *et al.*, ACS Appl. Mater. Interfaces **9**, 8194 (2017). Copyright 2017 American Chemical Society.

and wearable devices especially for 3D tissue engineering can be expected.[49] Reactive inkjet printing is a further developed *in situ* materials synthesis that combines inkjet printing with physical or chemical reactions. The advantages of reactive inkjet printing mainly focus on the precise control over the reaction site, the one-step scalable production, and the reduced material consumption. For the accurate *in situ* deposition of reactive inks, two inkjet nozzles can be closely integrated to eject different inks at the same point and at the same time, named "double-shot inkjet printing."[50] This "double-shot inkjet printing" can be extended to grow uniform single-crystal or polycrystalline thin films composed of compounds that are hardly soluble at the liquid–air interfaces.[51]

4. Pre-patterning

The inkjet-printed pattern's shape and resolution on a smooth homogeneous surface depend mainly on the behavior of droplets'

spreading and bonding. Pre-patterning the substrate before the inkjet printing process can fabricate complicated patterns with high resolution.[52] The pre-patterned hydrophobic and hydrophilic topology can provide driving forces that control the merging of the printed droplets as well as restrict the printing linewidth.[53] Takagi *et al.* reported the inkjet printing of aligned single-walled carbon nanotube (SWCNT) based transparent electrodes for flexible and wearable devices by self-assembled hydrophobic and hydrophilic contrast areas and boundaries.[54,55] Jiang and Kaminska introduced a structural-induced color technique by inkjet printing of transparent colorless titanium dioxide NPs on a pre-designed nanostructured-mold surface. Each layer of three vertically stacked polymer substrates had one specific subwavelength grating pattern, which showed primary colors of red, green, and blue. The diffractive colors with high-resolution inkjet printing were achieved by nanostructured surface pre-patterning that realized a full-color image as big as 10 × 10 cm^2.[56] Li *et al.* developed a solvent etching method to prepare surface-energy pre-patterns for suppressing the coffee-ring effects and programming the surface topology of depositions [Fig. 1(g)].[57] They etched hydrophobic patterns with ultrathin Cytop, which directed the inkjet-printed multilayered thin-film transistor (TFT) arrays of ITO/InGaO gates with an excellent average mobility of 7.4 $cm^2\ V^{-1}\ s^{-1}$.

D. High device flexibility/stretchability

The effective design with compatible modulus, high flexibility, and high stretchability for bearing the deformation caused by human motion is required in wearable electronics to fit the human body curvature. Conventional strategies that embed rigid components (sensors, chips, and circuits) in flexible substrates without effective connections can hardly fulfill the practical wearable demands.[58] Inkjet printing was regarded as a significant technology for the scalable production of all-flexible-component electronics. Developing the intrinsically flexible/stretchable inks (e.g., hydrogels) and the inks containing specific additives can improve the mechanical capabilities of inkjet-printed patterns. Apart from inks, the flexible/stretchable substrates are also desired because they can provide grounds for electrical element layout and protection and even perform some necessary parts of device functionality such as pressure detection and sweat component sensing.[59,60]

The commonly used rigid Si and SiO_2 substrates fail to meet the requirements of bendability, foldability, stretchability, and non-planar surfaces for wearable electronic systems. Hence, many new types of materials such as (thin) glass, metal (foils), papers, and polymers have been widely investigated as flexible substrates for inkjet printing.[61] Glass and metal foils with low thickness are bendable and can sustain very high sintering temperatures. However, the unfoldability, brittleness, and high expense of these inorganic substrates hinder their use in the fabrication of wearable electronics. Among all the flexible substrates, films and textiles based on paper and polymer are most favorable for next-generation wearable applications.[62]

1. Flexible/stretchable patterns

The inkjet-printed patterns should endure repetitive stress by avoiding breaking or disconnection, which causes electrical failure of the device. Several mechanisms that explain the failure of the inkjet-printed devices are based on physical and mechanical models:[63] (1) the effect of film edges, (2) cracking of printed patterns, and (3) interfacial slippage and delamination. When the printed film on the substrate is bent, the plastic components of the printed film will develop cracks to absorb the shear stress. The film edges of the cracked pattern will peel off from the substrates if the external stress exceeds the threshold limit. The device failure happens when the printed films fail to recover pristine electrical conductivity due to the formation of the cracks even after the external stress is withdrawn. As for the cracks and edge effect reduction, elastic rubber (elastomer) is considered as the optimal substrate to overcome these mechanical issues because of its relatively low Young's modulus, high viscoelasticity, and high stretchability compared with other polymers. Polydimethylsiloxane (PDMS), a typical low-cost elastomer, is widely used as a substrate for flexible and wearable electronic devices, thanks to its transparent, flexible, stretchable, and thermal resistive properties. The PDMS film can release the internal stress during the ink deposition process and distribute the stressed spots uniformly with the assistance of intentionally roughened surface.[64] Lee *et al.* demonstrated the inkjet-printing of crack-free Ag electrodes on pre-stretched PDMS substrates [Fig. 2(a)].[65] They found that previous issues of Poisson's effect and lateral cracks' formation on highly pre-stretched PDMS substrates can be effectively addressed by releasing the pre-stretched Ag electrodes on PDMS substrates and increasing the annealing temperature. To prevent disconnection inside the pattern films, flexible conductive materials were added to the ink or embedded in the PDMS substrates to endow the inkjet-printed patterns with high tensile-strain resistivity. Kim *et al.* demonstrated the inkjet printing of SWCNT electrodes, which were embedded inside the PDMS substrates with a normalized resistance of less than 1.2 after 1000 cycles under 100% tensile strain.[66] With the cross-linkable viscous rheological property of the elastomers, Jiang *et al.* realized "embedded inkjet printing" that directly sealed conductive microcables inside the liquid PDMS followed by a curing for encapsulation [Fig. 2(b)].[67] High-resolution silver lines of 1.6 μm and 1.7 aspect ratio were demonstrated for manufacturing highly flexible/stretchable devices with transparent multilayer integrated circuits.

A stable adhesion between the printed patterns (also cohesion) and substrates is necessary for inkjet printing of flexible/stretchable devices without slipping or delamination. The adhesion force between the ink materials and the substrate mainly depends on the morphology and chemical properties of the interface. Strategies such as physical and chemical modification of the substrate surfaces and the addition of another promotion layer for adhesion enhancement are commonly used. Self-assembled monolayer modified substrates were demonstrated to rapidly enhance the *in situ* interfacial adhesion in inkjet-printing by adsorbing and catalyzing the inks with tight bonding.[68] The interfacial fracture energy of the metal film is strongly affected by surface roughness and the mechanical interlocking effect. Lee *et al.* added a silane coupling agent in the inks as an adhesion promoter that utilized inorganic and organic reactivity in the same molecule to improve the adhesive strength for inkjet-printed patterns.[69] Qin *et al.* demonstrated that the thinner deposition of the palladium (Pd) film with higher surface energy would improve the interfacial adhesion toward various substrates. Inkjet printing of Pd thin films with a thickness of 100 nm was exhibited to have a stronger adhesive force with the

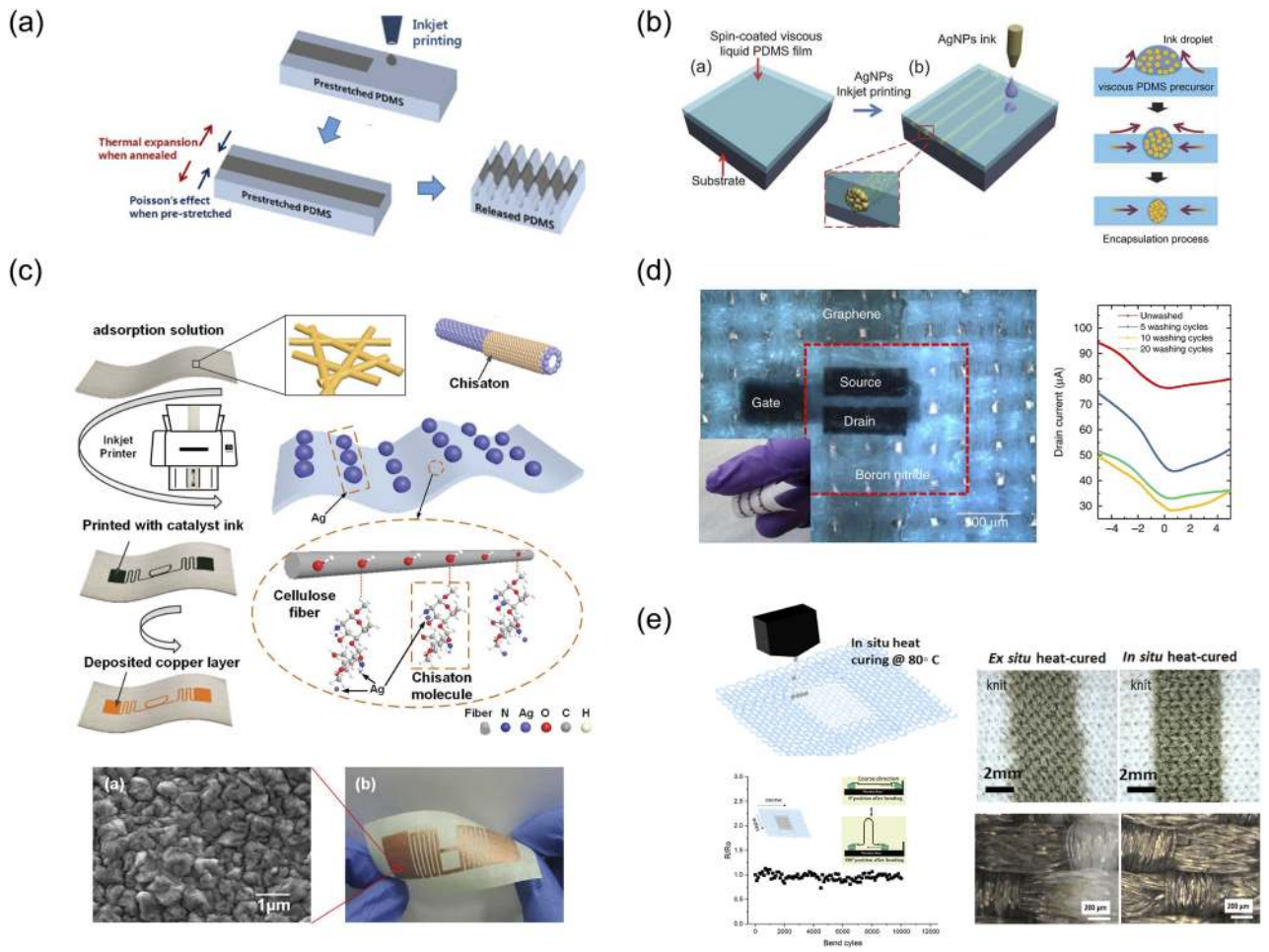

FIG. 2. (a) Inkjet printing of silver electrodes on pre-stretched PDMS substrates to reduce Poisson's effect and suppress lateral crack formation for wearable applications.[65] Reproduced with permission from Lee *et al.*, J. Phys. D: Appl. Phys. **46**, 105305 (2013). Copyright 2013 IOP Publishing Ltd. (b) Embedded inkjet printing of silver microcables inside PDMS and the sintering process of the ink droplet into the viscous liquid PDMS precursor.[67] Reproduced with permission from Jiang *et al.*, Adv. Mater. **28**, 1420 (2016). Copyright 2016 Wiley-VCH. (c) The fabrication process of a flexible paper-based metal antenna with inkjet printing of the protection layer and catalytic seeds.[73] Reproduced with permission from Wang *et al.*, Adv. Funct. Mater. **29**, 1902579 (2019). Copyright 2019 Wiley-VCH. (d) Left: all-inkjet-printed graphene/h-BN field-effect transistors on flexible polyester textiles with potential for wearable e-textiles. Right: the figure of drain current as a function of washing times.[75] Reproduced with permission from Carey *et al.*, Nat. Commun. **8**, 1202 (2017). Copyright 2017 Author(s), licensed under a Creative Commons Attribution 4.0 License. (e) Schematic of (up) conformal inkjet printing process to deposit a particle-free reactive Ag electrode on polyester textiles, which shows (down) almost unchanged resistance after 10 000 bending cycles.[76] Right: optical images (a comparison) of printed traces on textile knit between *in situ* and *ex situ* heat-curing processes. Reproduced with permission from Shahariar *et al.*, ACS Appl. Mater. Interfaces **11**, 6208 (2019). Copyright 2019 American Chemical Society.

PI substrates. Moreover, the air-plasma-treated PI substrates also showed improved adhesion from the reactive oxygen-containing groups and nitrogen-containing groups brought by the plasma treatment.[70]

2. Flexible/stretchable substrates

Polymer plastic substrates for inkjet printing mainly include semi-crystalline plastics such as polyethylene terephthalate (PET), polyethylene naphthalate (PEN), polyetheretherketone (PEEK), and amorphous plastics, e.g., polyvinyl chloride (PVC), polycarbonate (PC), and polyethersulfone (PES). Semi-crystalline plastics have a defined melting temperature (T_m) above which the plastics rapidly change from rigid to a flexible state, whereas amorphous plastics have a melting range related to the glass-transition temperature (T_g) and softens as the temperature rises in this range. The main issue of polymer plastic substrates is their generally low T_g and T_m (Table I, typically <300 °C), which makes them easily deform or melt in the sintering process of inkjet printing (typically >300 °C). Only some expensive plastics with a high thermal performance such as polyimide (PI) (T_g between 360 °C and 410 °C) are capable of surviving such high temperatures. Many strategies were developed to decrease the sintering temperature such as flashlight sintering,

TABLE I. The T_m and T_g of typical plastic substrates for flexible electronics.

Semi-crystalline plastics	T_m (°C)	Amorphous plastics	T_g (°C)
PET	245–265	PVC	65–85
PEN	260	PC	140–150
PEEK	330–340	PES	220–230

chemical sintering, microwave sintering, electrical sintering, plasma sintering, and photonic sintering. Furthermore, sinter-free metal reactive ink was also potential for inkjet printing on various substrates and will be discussed in the section of metallic material-based inks.

In addition to polymer film substrates, paper is also widely adopted as a flexible substrate for inkjet printing because of its lightweight, cost-effective, designable, and portable characteristics for biodegradable electronics.[71] However, the porous cellulose-based networks of paper tend to absorb the liquid inks, forming an unmanageable deposition with a lowered resolution as well as bad electrical property. Surface modification such as omniphobic treatment that utilized interfacial free energy was reported to enable high-resolution inkjet printing on paper substrates.[28] A plasma-assisted inkjet printing approach was also developed for highly conductive metal deposition on paper at room temperature and atmospheric pressure without sintering.[72] This plasma-assisted process overcame the unwanted wetting effect by quick deposition of the metallic layer on paper and prevented ink penetration into the porous paper fibers. Wang *et al.* proposed inkjet printing of flexible metal antennas for paper-based radio-frequency identification devices with the assistance of surface modification and electroless deposition (ELD). To avoid ink penetration and wetting issues, the paper-based substrate was first modified with a gel film and a chitosan adhesive layer using the $SnCl_2$ colloidal solution. Then, the catalytic seeds for metal deposition were inkjet-printed on the protection gel film. The subsequent ELD of conductive metal antenna deposition was performed to form an elaborated copper antenna layer on paper [Fig. 2(c)].[73]

Textile substrates with both flexibility and stretchability provide a promising platform for the integration of electronics into clothing and bring more comfortable wearing experiences than rigid wearable substrates. Although inkjet printing on textiles is widely used in the garment industry for dyeing, the printing of continuous and high-resolution patterns for electronic devices is still challenging on textile substrates. The major problems of the inkjet printing on textile-based materials concern the quality of deposited ink trace that depends on the tightness, diameters, porosity, and surface energy of the curved textile fibers. Karim *et al.* first reported the inkjet printing of graphene on pre-treated textiles with organic NPs for all-inkjet-printed textile-based wash-stable electronic devices. The pre-treatment layer on textiles acted as the reduced graphene oxide (rGO) reception layer for accurate deposition of conductive tracks by inkjet printing in a rapid, scalable, and low-temperature processing.[74] Carey *et al.* demonstrated the all-inkjet-printed graphene/hexagonal-boron nitride (h-BN) field-effect transistors (FETs) on flexible polyester textiles that showed great potential for wearable e-textiles and flexible circuits at room temperature [Fig. 2(d)].[75] This textile-based inkjet-printed device reached an average field-effect mobility of 91 ± 29 $cm^2\ V^{-1}\ s^{-1}$, which was a magnitude larger than the inverted-staggered heterostructure using the spin-coating process. Moreover, by pressing a waterproof polyurethane-protective layer on the textiles, as-prepared FETs can be water-washed for over 20 times without significant degradation. Notably, the deposition of conformal metal NPs' coating on wearable textiles is also challenging because of problems such as interfacial delamination, bad conductivity, and cracking issues. Shahariar *et al.* proposed a novel conformal inkjet printing process of depositing particle-free reactive Ag inks on polyester textiles in one step [Fig. 2(e)].[76] This process was followed by an *in situ* heat-curing process that minimized the wicking of the ink into textile structures and created a conductive network coating on an individual fiber. The conductivity of the as-prepared pattern on the knit fabric only lost half of the original value after 15 washing cycles and remained almost unchanged after an unprecedented 10 000-bending-cycle test. Kim *et al.* proposed that inks penetrated more deeply into jersey/interlock knit through interstices of textile fibers, and therefore, the thin conductive layers by *in situ* annealing would yield continuous electrical pathways.[77] Higher electrical conductivity by the particle-free inkjet printing was attributed to no agglomerations near the jetted side of fiber, which prevented disconnections and non-uniformity of the deposited metal. Inkjet-printed textile-based technology is foreseen as a promising future platform for consumer products of wearable electronic devices with wearability, washability, and breathability.

III. FUNCTIONAL INKS FOR INKJET PRINTING

Various ink materials including polymer, metal, carbon, and, in particular, the surging hydrogels and 2D materials, have been investigated for inkjet printing. In this section, we will discuss different functional materials for inkjet-printed flexible/wearable electronics and material properties for high-performance design, as well as strategies to overcome technical limitations of specific materials. A summary of recently reported functional inks concerning the ink property (functional material, solvent, and printing related parameters), the substrates (with corresponding sintering temperature), and the electrical properties (with device applications and advantages) is given in Table II.

A. Organic polymer-based inks

Printing of organic polymer-based inks only involves solvent processing at ambient conditions instead of high annealing temperature for printing inorganic materials. The intrinsic flexible and stretchable properties endow the organic polymer-based electronic devices with extra functionality and good reliability toward the movement of the human body. The high compatibility of organic polymer-based inkjet printing on various plastic substrates also makes it attractive for flexible circuits, sensors, and bio-applications.[78] Despite relatively modest operational speed compared with Si- and other inorganic-based materials, devices based on polymeric semiconductors provide excellent flexibility, lightweight, low cost, and high-throughput manufacturing. Recent developments of donor–acceptor (D–A) conjugated polymers with anisotropic transport such as diketopyrrolopyrrole (DPP), naphthalenediimide (NDI), and isoindigo (IID) have promoted polymeric semiconductor to an impressive mobility of >20 $cm^2\ V^{-1}\ s^{-1}$.[79–81]

TABLE II. Summary of recent progress on functional inks for inkjet printing.

Ink material	Solvent	Substrate and sintering temperature	Ink and printing parameter	Electrical property	Application	Reference
			Organic polymer-based inks			
P(NDI2OD-T2)	Mesitylene	...	$R_e \approx 2.3$	Mobility ≈6.4 $cm^2\ V^{-1}\ s^{-1}$ at 3.3 MHz	Printed FETs operating in the MHz regime and radio-frequency identification tags	82
P3HT/PS	*O*-dichlorobenzene	Au/SiO_2	...	Mobility > 1 $cm^2\ V^{-1}\ s^{-1}$ and on/off ratio $>10^7$	Source–semiconductor–drain coplanar transistor for OFETs of high on/off ratios	84
Polymethylsilsesquioxane	Alcohol	PET, ≤150 °C	Viscosity of 11 cP	Dielectric constant ≈3	Flexible bottom-contact top-gated *n*-type transistors with low current leakage	93
			Metallic material-based inks			
Ag NPs/NaCl	Propylene glycol/water	PET, room temperature	...	Resistivity of 16 $(\pm 2.2) \times 10^{-6}\ \Omega$ cm	"Self-sintered" metal dispersion for thermal-sensitive plastic-based wearable electronics	96
Ag–Ga–In liquid alloy	...	Paper, room temperature	...	Conductivity of 4.85×10^6 S m^{-1} (gauge factor ≈ 1)	Stretchable circuits (above 80% strain) on 3D surfaces and soft on-skin electronic tattoo	97
Silver ammonia and formaldehyde	Water	Polymer substrates, ≤150 °C	Viscosity of 1.02 cP	Resistivity of 12 $\mu\Omega$ cm	Dual-channel reactive printing for embedded wearable circuits and micro-electromechanical systems	98
			Carbon-based inks			
Graphene/nitrocellulose (ethyl cellulose)	Cyclohexanone/terpineol	PET and PEN	Viscosity of 10 mPa s–15 mPa s	Conductivity of 2.5×10^4 S m^{-1}, capacitance of 0.14 mF cm^{-2}	Printed solid-state graphene microsupercapacitors on flexible and thermal-sensitive substrates such as glassine paper	103 and 104
Graphene/MWCNTs	Water	Paper	Force constant of 20 N m^{-1}–75 N m^{-1}	Conductivity of 1.4×10^4 S m^{-1}	Flexible and stretchable PVA/graphene/MWCNT composite electrical wire	105

TABLE II. (*Continued.*)

Ink material	Solvent	Substrate and sintering temperature	Ink and printing parameter	Electrical property	Application	Reference
			2D material-based inks			
Organohalide 2D perovskite	DMF	PI	...	Photoresponsivity ~0.17 A W^{-1} and on/off ratio ≈ 2.3×10^3	Heterostructured flexible photodetector devices with high response speed	111
h-BN/graphene	NMP/ethanol	Polyester textile, room temperature	Z of 19.4–22	Mobility of 150 (± 18) cm^2 V^{-1} s^{-1}	Fully inkjet-printed, washable, and flexible complementary inverters, logic gates, and rewritable volatile memory	75
$MoSe_2$, MoS_2, WSe_2, and WS_2 nanosheets	NMP/isopropanol	PET	Z of 17	Transconductance > 5 mS and mobility > 0.1 cm^2 V^{-1} s^{-1}	All-printed porous nanosheet network-based flexible TFTs at low driving voltage	113
			Hybrid/nanocomposite material-based inks			
BST@PMMA composite	Butyl diglycol/butanone	PET, 60 °C	Z of 6–17	Dielectric constant of 20–55	Fabricating composite thick and multilayer films for wearable electronics or smart packaging	119
AuNPs @ PEDOT:PSS	Water	Cardboard and paper	Z of ~7	Resistivity of 5.2 (±0.4) × 10^{-3} Ω cm	Repairing electrodes' cracks from bending or folding or to recover them from the wearable devices	122
$BaTiO_3$ @ epoxy	DMF	PI	...	Dielectric constant of 92	All-inkjet-printed wearable piezoelectric energy harvester	123

Caironi's group reported the combination of multiple depositing methods with inkjet printing to synthesize a highly controlled submonolayer of semiconducting P(NDI2OD-T2) and conducting poly(3,4-ethylenedioxythiophene) polystyrene sulfonate (PEDOT:PSS) on a plastic substrate for a dielectric layer and gate electrode, respectively. The printed all-polymer FET featured a record-high transition frequency of larger than 14 MHz (at a bias voltage of 7 V), which was demonstrated to operate in a rectifying circuit with a 13.56 MHz near-field communication (NFC) wireless chip.[82,83] For inkjet-printed FETs, the polymeric semiconductor–insulator bilayer structure benefits the charge transport, but the source–drain current and charge injection within the channel are confined due to the impediment of the insulating layer. Bu *et al.* developed a one-step inkjet printing of source–semiconductor–drain coplanar FETs with vertical phase segregation of poly(3-hexylthiophene)/polystyrene (P3HT/PS) inks

as a semiconductor–insulator bilayer. The organic polymer-based printing in a coplanar semiconductor–insulator bilayer transistor enlarged the injection area and passivated the insulating dielectric layer, thus enhancing the overall transistor performance [Fig. 3(a)].[84] Conductive polymers such as poly (3,4-ethylenedioxythiophene) (PEDOT), polypyrrole (PPy), and polyaniline (PAni) are widely adopted as inkjet-printed electrode materials owing to their tunable viscosity, excellent stability, and high conductivity.[85–89] The electrical conductivity and charge transfer of organic polymers are attributed to the delocalized π electrons of overlapped p-orbitals from the conjugated system in the polymer backbone. Water-dispersed PEDOT:PSS can reach up to 4000 S cm^{-1} conductivity under 100% strain even though the doping of hydrophilic PSS is difficult.[90,91] Yano *et al.* developed a new self-doped highly conductive PEDOT (S-PEDOT) (~1089 S cm^{-1}) that can be dissolved in water and various organic solvents as polymer-based ink for inkjet printing.[92]

In particular, inkjet printing of conductive hydrogel with good biocompatibility has been a hotspot within wearable health-monitoring electronic devices. Various bio-sensors with interfacial engineering would be discussed later, which build the bridge between electronic activities and the human body (organs and tissues). Inkjet-printed conductive hydrogels showed tailorable conductivity with different carriers (electronic, ionic, or hybrid). The

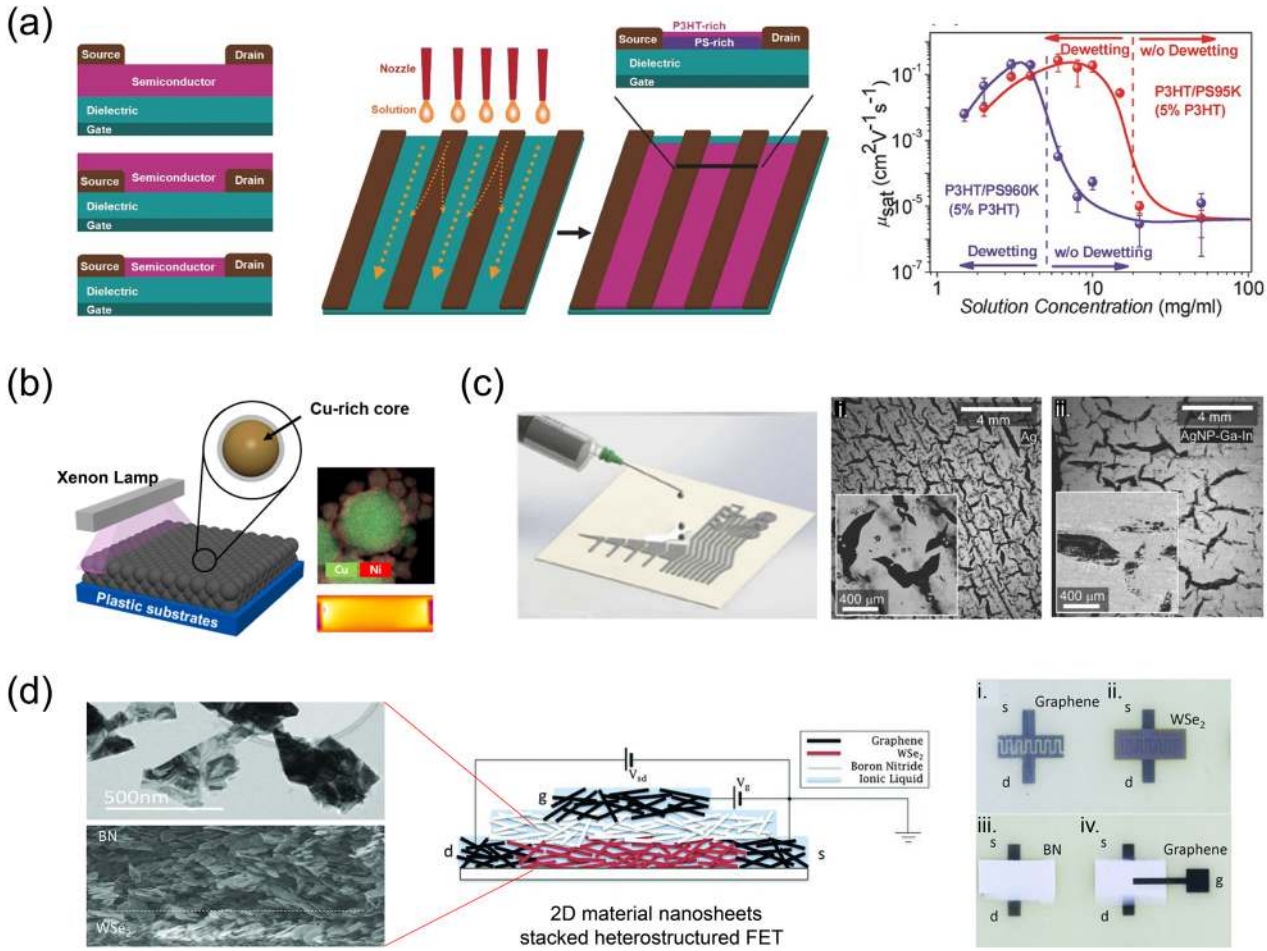

FIG. 3. (a) Left: schematic of the inkjet-printed field-effect transistor with vertical poly(3-hexylthiophene)/polystyrene as semiconductor/insulator bilayers to enhance the overall transistor performance. Right: dependence of saturated mobility on the concentration of polymer solution.[84] Reproduced with permission from Bu *et al.*, Adv. Mater. **30**, 1704695 (2018). Copyright 2018 Wiley-VCH. (b) Flash photonic sintering of printed Cu@Ni metallic NPs on various polymer substrates at low temperatures.[95] Reproduced with permission from Kim *et al.*, ACS Appl. Mater. Interfaces **10**, 1059 (2018). Copyright 2018 American Chemical Society. (c) Liquid alloy sintering method of melting inkjet-printed Ag particles into AgNP–Ga–In liquid alloy coating. Right: SEM image of inkjet-printed Ag films before and after sintering.[97] Reproduced with permission from Tavakoli *et al.*, Adv. Mater. **30**, 1801852 (2018). Copyright 2018 Wiley-VCH. (d) Middle: schematic of the all-inkjet-printed thin-film transistor based on two-dimensional (2D) semiconducting materials with graphene electrodes, a transition metal dichalcogenide (e.g., WSe_2) channel, and a boron nitride (BN) separator. Left: TEM and SEM images of 2D materials and heterostructures. Right: photographs of the inkjet printing steps [from (i) to (iv)].[113] Reproduced with permission from Kelly *et al.*, Science **356**, 69 (2017). Copyright 2017 American Association for the Advancement of Science.

physicochemical properties of printed hydrogels (e.g., modulus, toughness, and rheological properties) can also be controlled for specific functionalities such as shape memory, self-healing, and surface adhesion. Moreover, organic polymers can act as a binder or additive to adjust the viscosity of the ink. Electrical insulating polymers such as PVP, PI, PET, polypropylene (PP), polyvinyl alcohol (PVA), and polystyrene (PS) are conventionally deposited as a dielectric layer or passivation layers for inkjet-printed organic thin-film transistors.[52] Dadvand *et al.* demonstrated three-layer flexible *n*-type transistors based on the inkjet printable polymethylsilsesquioxane-dielectric film with picoampere leakage current at even 60 V operation voltage.[93] The significant advantage is that the contiguous metallic gate electrode and semiconducting material layer would not react with the polymer-based dielectric layer due to relatively low cross-linking temperatures (<150 °C) of all-methyl silsesquioxane. Owing to the high editability of polymer hydrogels, many novel printing methods were developed to enhance inkjet printing. For example, Yoon *et al.* reported a hybrid bioprinting strategy that integrated spray coating with inkjet printing for the fabrication of different biocompatible hydrogels with controllable shapes including alginate, cellulose nanofiber, and fibrinogen. The cross-linking reagents were sprayed onto the inkjet-printed gelatine methacryloyl/sodium alginate (GelMA/NaAlg) sample at high speed and induced the polymerization of a large-scale hydrogel structure (>10 cm) that mimicked human tissues.[94]

B. Metallic material-based inks

Inorganic metallic materials exhibit favorable mechanical and chemical properties that make the inkjet-printed devices stable under various conditions, such as high temperature, high humidity, and a corrosive environment. Au is the most bio-compatible candidate with chemical inertness for the long-term use of *in vivo* devices and contact interface with the body. Silver-based bonding wires are the most commonly used connections in flexible and wearable electronics due to high electrical conductivity with good ductility and processability. Al and Cu are also commercially employed for their low price and favorable electrical properties, but they are easily oxidized. Kim *et al.* reported a sequential solvothermal synthesis to coat the Ni protective shell over the conductive Cu nanoparticle, which endowed the Cu nanoparticle-based electrode with oxidation resistance and stability even at 200 °C under 85% relative humidity [Fig. 3(b)].[95] A flash photonic sintering was performed under air ambient conditions with no reducing gas. In most cases, the inkjet printing of metal requires metallic NPs or organometallic precursors dissolved in water or organic solvents with stabilizers, followed by sintering post-processing. However, the high temperature of the sintering step may damage the polymer components or flexible electronic substrates as discussed above. For the printing on flexible substrates, low-temperature sintering methods of metallic inks were adequately investigated. Grouchko *et al.* presented a concept of a built-in sintering mechanism that used a sintering agent (such as NaCl) to destabilize the inkjet-printed metallic composites and enhance 41% conductivity.[96] Sintering could be operated with no heating because the ions of NaCl replaced and detached the stabilizers' groups on the metallic NPs and coalesced them into continuous electrical contacts. Tavakoli *et al.* proposed a liquid alloy sintering method using eutectic gallium–indium (EGaIn) to melt inkjet-printed Ag particles into Ag–Ga–In liquid alloy coating at room temperature [Fig. 3(c)].[97] As-printed Ag–Ga–In circuits on tattoo papers exhibited six orders of magnitude increase in volumetric conductivity from 3.6×10^6 S m^{-1} to 4.85×10^6 S m^{-1} compared with un-sintered Ag circuits. Other sintering approaches such as chemical sintering, microwave sintering, electrical sintering, and plasma sintering also allow the precise and local heating of the ink in a short period. The thermal energy transferred from NPs to the substrate can be effectively controlled within the permissible limits, but the high cost and limited operation conditions impeded their large-scale applications. Besides, the use of particle-free metal reactive inks is also an alternative way to lower the sintering temperature and avoid stabilizers. Kao *et al.* designed a dual-channel drop-on-demand inkjet reaction system, of which silver ammonia solution and formaldehyde solution were filled in two neighboring ink cavities, to print continuous silver circuit lines of 200 nm width.[98] The sintered Ag showed the conductivity of 7.5 times higher than that of bulk silver after reaction of sequential drops from two channels at the same position.

C. Carbon-based inks

Carbon-based materials such as carbon nanotubes (CNTs), graphite flakes, and graphene are compatible with inkjet-printed flexible and wearable electronics because of their versatile properties such as excellent mechanical strength, high chemical stability, easy processing, and controllable electrical conductivity (metallic or semiconducting properties). The pristine carbon-based materials show a strong hydrophobic nature due to the aromatic and non-polar structure that has bad dispersion in water and other polar solvents. The organic solvents such as dimethylformamide (DMF) and *N*-methylpyrrolidone (NMP) have very low dispersity (<0.1 mg mL^{-1}) and require high sintering temperature for removal of organic residues that may damage the carbon structure. For the long-term dispersibility of carbon in an aqueous solvent, chemical surface-modification was proved to be more effective than mechanical approaches such as ultrasonic dispersion and high-shear mixing. The surface wettability of carbon can be altered from hydrophobic to hydrophilic after the simple oxidization or functionalization with hydrophilic groups, such as carboxyl, hydroxyl, and amide groups.[99] Alternatively, noncovalent functionalization via π–π stacking interaction was also employed to promote the dispersibility, the thermal conductivity, and the optical properties while preserving the electrical performance, which was convinced by temperature-variable NEXAFS spectra of the π-electron cloud systems.[100] Lu *et al.* reported an excellent solution-processable multi-wall carbon nanotubes (MWCNTs) attached by binaphthylamine-based hole-transport molecules, which were potential for inkjet-printed wearable perovskite solar cells.[101] Díez-Pascual's group reported the PEDOT:PSS grafted GO reinforced with hexamethylene diisocyanate by a straightforward solution casting method and realized a functionalization degree of 18.1%.[102] Generally, most of the commonly used surfactant dispersion can be grafted into carbon-based materials with a simple solution process including sodium dodecyl sulfate (SDS), sodium dodecyl benzenesulfonate (SDBS), hexadecyltrimethylammonium bromide (CTAB), and amphiphilic copolymers. To decompose these surfactants, high processing temperature is usually required in traditional

thermal annealing, which is not compatible with temperature-sensitive substrates. Hersam's group demonstrated a rapid pulsed light annealing for inkjet-printed graphene ink mixed with exothermic polymer binder nitrocellulose as annealing reaction's energy source.[103] The pulsed light annealing enabled a highly porous microstructure and low processing temperatures with broad process compatibility in versatile liquid-phase processing of graphene inks on flexible substrates.[104] Moreover, a non-surfactant way of pristine graphene dispersion in water was proposed by Georgakilas *et al.* through the self-assembly with hydroxyl functionalized CNTs that overcame the incomplete functional groups' coverage of the nanosheet surfaces.[105] This method provided well dispersed (up to 15 mg mL^{-1} in water) graphene sheets wrapped by hydrophilic CNTs for highly conductive graphene inks in inkjet printing. The bandgap of metallic and semiconducting SWCNTs ranged from 0.4 eV to 2.0 eV according to their chiral structures, while the MWCNTs could even show 0 eV bandgap and a current density of 10^9 A cm^{-2} for high-performance wearable electrodes or circuit applications. Other alternative routes toward high-concentration or surfactant-free carbon dispersion such as solvent exchange, liquid-phase exfoliation, and oxidization–reduction processes are also promising for high-quality printing.[106,107] Moreover, when the deposition thickness and density of the materials are decreased, the inkjet-printed CNTs and graphene film would exhibit an optical transparency feature.

D. Two-dimensional (2D) material-based inks

2D (van der Waals) materials with only single or few layers of atoms have drawn much attention over the past few decades. Atomic-thin 2D materials with monolayer structures, such as graphene, transition metal dichalcogenides (TMDCs), black phosphorus, metal carbides, nitrides, and carbonitrides (MXenes), show intrinsically distinct properties over their bulk structures. Inkjet printing of 2D materials is promising for next-generation flexible and wearable electronics because of their unique structure-derived (electrical, mechanical, optical, and thermal) properties.[108] For example, graphene as mentioned above has much enhanced electrical and thermal conductivity because of the quasi-2D electron and phonon transport in a honeycomb lattice. The large surface-to-volume ratio of 2D manganese dioxide offers a high specific surface area, an efficient electron transfer path, and fast carrier mobility, which benefit the applications such as pseudocapacitive energy storage. Specifically, the direct van der Waals heterojunction based on different 2D materials is allowed by inkjet printing of vertically multiple-layer stacked heterostructures for FETs and optoelectronics.[109] Moreover, the nature of excellent biocompatibility, high chemical stability, outstanding flexibility, and good transparency make 2D materials compatible with the liquid-phase printing process for high-performance wearable applications. Withers *et al.* combined different methods (such as drop-casting and vacuum filtration) with inkjet printing for low-cost and scalable fabrication of complex heterostructures such as BGr/WS_2/TGr.[110] Min *et al.* demonstrated inkjet printing of 2D organohalide heterostructured flexible photodetector (PD) $(CH_3(CH_2)_3NH_3)_2(CH_3NH_3)_{n-1}Pb_nI_{3n+1}$ (n = 2, 3, and 4) on PI substrates. The reported PDs with controllable layer-by-layer deposition size had better environmental stability than spin-coating processed ones.[111] In addition, 2D materials can be dispersed in some solvents with a high boiling point (>100 °C) without stabilizers, such as NMP and DMF, due to the matching of the Hansen solubility parameters. However, the high annealing temperature in post-processing for these solvent removals may damage the plastic or textile's flexible substrate. Zhou *et al.* reported a mixed-solvent strategy using two-solvent mixtures composed of ethanol/water to simultaneously lower the boiling point and maintain the affinity of the solvent toward the 2D materials.[112] A solvent exchange method was reported for graphene/hexagonal-boron nitride (h-BN) ink preparation, whereby 2D layered materials were exfoliated at high speed in the high boiling point solvent and suspended at the low boiling point solvent with desired concentration. NMP was exchanged to ethanol for a 2D material solvent that facilitated the evaporation at ambient temperature and then formulated the ink with Z ~ (19.4–22) as the optimal Z range for a high-uniformity heterostructure on polyester textile.[75] Recently, inkjet printing of TMDCs for all-printed, vertically stacked 2D TFTs has attracted researchers' interest. Contrary to zero-bandgap graphene, the bandgap of MoS_2 can be tuned by stacking different layers (~1.3 eV for multilayer and ~1.8 eV for monolayer), which allows photogeneration and recombination with high efficiency. Kelly *et al.* investigated a variety of 2D semiconducting materials such as $MoSe_2$, MoS_2, WSe_2, and WS_2 by liquid-phase exfoliation in the NMP solvent for channel deposition of 2D TFTs [Fig. 3(d)].[113] The inkjet-printed 2D nanosheet network channels reached an on/off ratio of up to 600, a high transconductance of over 5 mS, and a competitive charge-carrier mobility of >0.1 $cm^2\ V^{-1}\ s^{-1}$, which allowed operation with high currents at relatively low driving voltages. Moreover, the inkjet printing of 2D materials has also been developed to fabricate alternative flexible and wearable electronics such as electromagnetic shields, photodetectors, and flexible supercapacitors, which are promising in highly integrated systems for flexible and wearable electronic applications.[114,115]

E. Hybrid/nanocomposite material-based inks

The use of organic–inorganic hybrid nanocomposites in inkjet printing can exploit the advantage of versatile functional nanomaterials on flexible substrates. The hybrid/nanocomposite materials such as carbon/polymer-based hybrids, metal/conducting polymer nanocomposites, and inorganic semiconductor/organic semiconductors not only showed metrics of individual components but also exhibited synergic-effect reinforced properties of mechanical robustness, electrical conductivity, optically transparent, and magnetic response.[116,117] For example, to improve the electrical performance of printed inorganic materials, a hybrid nanocomposite network can be built by a physical or chemical cross-linked conducting polymer that is compatible with the inkjet printing process. After embedding the functional inorganic materials (such as MXenes, Si, and Fe_2O_3) into the conducting polymer-based matrix, the hybrid materials will show better electrical properties such as enhanced electrochemical performances.[118] Moreover, with the assistance of hybrid materials, some ingenious strategies were also developed to solve some specific issues in the inkjet printing process. Mikolajek *et al.* used the ceramic/polymer [$Ba_{0.6}Sr_{0.4}TiO_3$/poly(methyl methacrylate)] composite inks to fabricate thick homogeneous dielectric films via layer-by-layer inkjet printing on flexible PET

substrates.[119] The hybrid ink system had an improved drying behavior over the pristine ceramic and therefore showed much higher structure homogeneity. Hybrid/nanocomposite material-based inks can also prevent the coffee-ring effect of the thin dielectric layer below 1 μm by instant polymerization and stabilization of the ink upon reaching the heated substrates.[120] The combination of the high dielectric constant of ceramics and the edible functionality of polymers provided wide applications in flexible and wearable electronics. Kraus *et al.* reported the concept of sinter-free electronic inks by coating metal or semiconductor NPs with a 1 nm layer of conducting polymers and the formed core–shell nanocomposites for inkjet printing.[121,122] With the π–π stacking of conductive layers, the nanocomposite particles could form interpenetrating conducting routes on substrates upon drying, with no need for the high-temperature sintering. Lim *et al.* demonstrated the all-inkjet-printed piezoelectric $BaTiO_3$/resin hybrid deposition on a flexible substrate with no cracks or phase separation after the sintering process. Owing to the high mechanical robustness of the hybrid nanocomposite resin, the film could sustain 2000 continual bending cycles and maintained an output voltage of ~7 V, which was promising for future wearable energy harvesters.[123]

IV. FLEXIBLE AND WEARABLE ELECTRONIC DEVICES

With elaboration on ink materials, substrates, and printing strategies, inkjet printing demonstrated the reasonable potential of implementing various functions for advanced wearable applications. Cases of recently reported inkjet-printed flexible and wearable electronics are summarized and highlighted in this section, including sensors, displays, transistors, energy storage devices, and some other devices.

A. Flexible and wearable sensors

1. Biosensors

Wearable biosensors emerged as the novel platform for health monitoring and disease diagnosis via human metabolite analysis.[7,124–126] Samplings of biofluids, such as tears, sweat, saliva, interstitial fluids, and blood, are often utilized to measure the concentration of the metabolic biomarkers that closely correlate with the human physiological status. A competitive approach for wearable biosensors with high selectivity and quantitative capability is the electrochemical analysis based on enzymatic reactions in response to particular molecules including glucose (Glu), lactate (LA), urea, and ethanol. For example, glucose oxidase (GO_x) is a widely adopted enzyme family for glucose metabolism, in which reaction products (e.g., H_2O_2) or electron exchange is detected in response to the target substrate of glucose. Inkjet printing is capable of meeting the challenges for wearable biosensors' scalable fabrication where cost-efficiency and pattern precision are extensively concerned. On the one hand, the DoD strategy minimizes the consumption of expensive enzyme slurry through selective drop deposition onto the working areas. On the other hand, the inkjet process can pattern multilayer enzymes and conductive materials without masks or complex alignment. Exerting the uniform and scalable characteristics, inkjet-printed wearable biosensors are promising for various bio-sensing and health monitoring applications.

The amperometric method, which relies on the three-electrode electrochemical system, can detect the concentration of biomarkers by measuring the current intensity in the enzymatic electrochemical reaction. Stable immobilization and high loading capacity of the enzyme on working electrodes are crucial factors for printable amperometric wearable biosensors with good durability and sensitivity. Li *et al.* utilized the PAni hydrogel as the interfacial materials that provided both biocompatible hosting matrix and electrical connection for printed enzymes [Fig. 4(a)].[127] An all-inkjet-printed amperometric biosensor was demonstrated with multiplex microfluidic channels for the detection of triglycerides (TG), lactate, and glucose. Hydrogel precursor solutions were inkjet-printed on screen-printed carbon current collector units where the hydrophilicity difference of the PET substrate was predefined as printing footprints. Next, sequential inkjet printing of catalyst platinum nanoparticles (PtNPs) and multiple enzyme solutions was performed to modify the PAni hydrogel electrode layer. Principally, the amperometric measurement was conducted based on detecting electrons from PtNP-catalyzed oxidization of H_2O_2, which was generated from enzymatic reactions. In the multiplex electrochemical detection, good sensitivity and high selectivity were achieved simultaneously due to the efficient molecular diffusion and electron transportation along with the high loading density of the PtNP catalyst in the porous conductive hydrogel matrix. Taking advantage of the direct printability on arbitrary surfaces of inkjet printing, Pu *et al.* proposed an inkjet-printed cylindrical working electrode for implantable glucose biosensing.[128] The rGO/Au inks were first inkjet-printed as the conductive working electrodes onto the pre-treated hydrophilic surface of the flexible polyetheretherketone rod with 1 mm diameter. After thermal annealing, PtNP ink for catalyzing H_2O_2 oxidization, Nafion solution for immobilization, and GO_x enzyme were separately inkjet-printed and modified on the rGO/Au electrode. The surface area of the cylindrical working electrode was increased, and thus, the sensitivity for accurate clinical detections was improved even under hypoglycemia conditions. In addition to monitoring byproducts from the enzymatic reactions, enabling direct electron transfer (DET) between electrodes and enzymes is another approach of improving biosensing efficiency and interference immunity. Nanomaterial-based electrodes, such as nanomesh of SWCNTs,[129] exhibited promising biosensing capacity for their large surface area to accommodate biomolecule loadings and comparable dimensions to interconnect redox centers with electrodes. Kang *et al.* demonstrated an inkjet-printed DET-based glucose biosensor by preparing SWCNT-M13 phage ink on the working electrode.[130] The amphiphilic M13 phage served as the negatively charged template to enable stable bonding with SWCNTs and ionic compatibility. GO_x ink was then inkjet-printed and electrostatically coupled with the electrode by using the polyelectrolyte interlayer of polyethylenimine. Good printability, electrochemical coupling, and hydrostability were achieved through the optimization of nano-sized bio-ink and printing conditions. The robust biosensor assembled on a paper substrate showed a low detection limit of glucose concentrations at 20 μM, which was promising for wearable sensing applications.

Another commonly adopted architecture for inkjet-printed biosensors is the electrochemical transistor, in which a gate electrode was used to load and immobilize enzymes. Selective oxidization of the target analyte by the gate electrode can

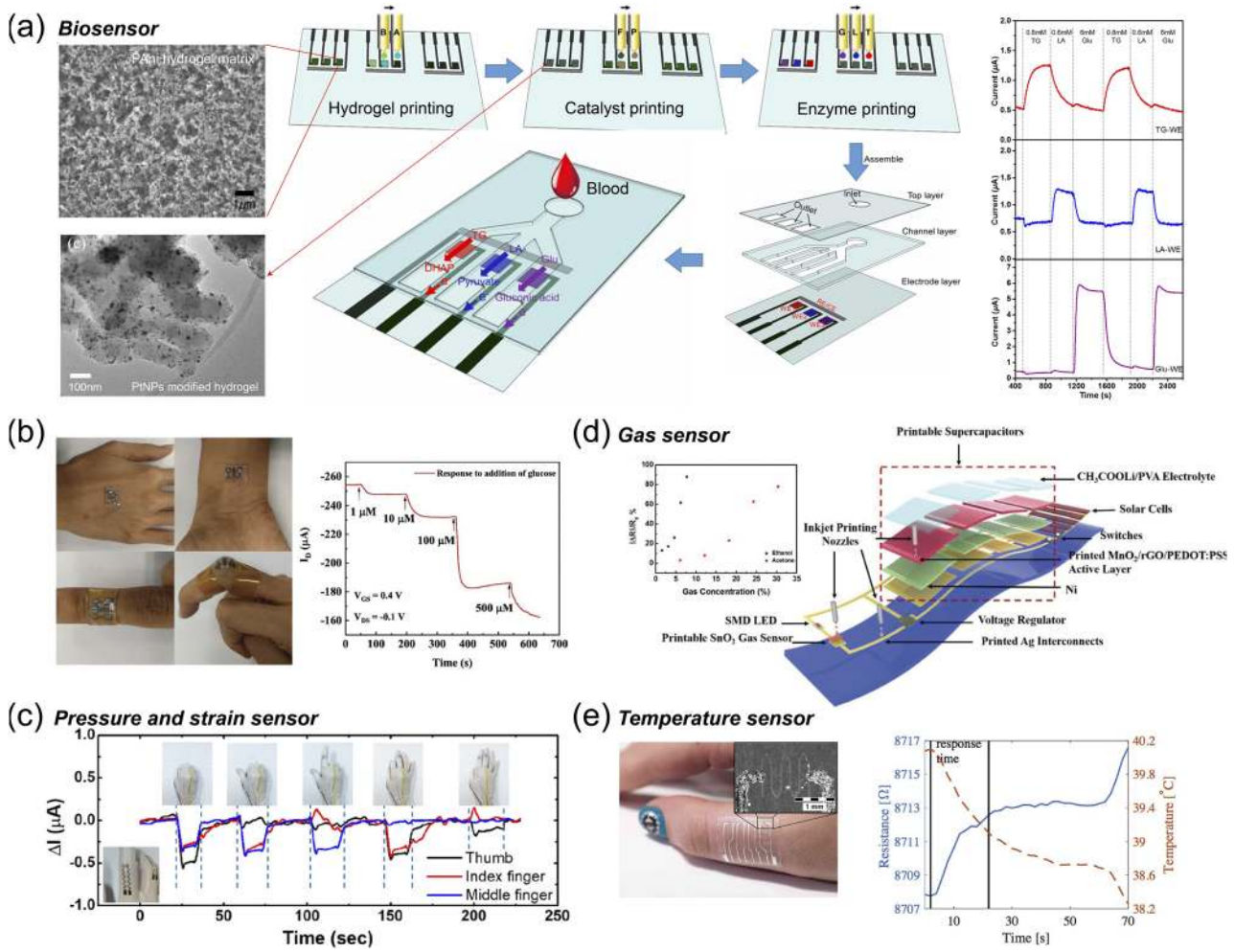

FIG. 4. (a) Middle: schematic illustration of printable fabrication procedures of the all-inkjet-printed amperometric biosensor with a multiple-enzyme-based working electrode for detection of triglycerides (TGs), lactate (LA), and glucose (Glu). Left: SEM and TEM of the hydrogel matrix and the loading of PtNPs, respectively. Right: current–time curves of detecting metabolites with the multiplexed essay.[127] Reproduced with permission from Li *et al.*, Nano Lett. **18**, 3322 (2018). Copyright 2018 American Chemical Society. (b) Demonstration of an organic electrochemical transistor with inkjet-printed Pt and GOx inks and measurement of glucose concentration.[132] Reproduced with permission from Li *et al.*, Adv. Electron. Mater. **5**, 1900566 (2019). Copyright 2019 Wiley-VCH. (c) Responses of inkjet-printed piezoresistive mechanical sensors to various hand motions. Different hand motions produced a unique pattern of resistance levels.[137] Reproduced with permission from Kang *et al.*, Nano Lett. **19**, 3684 (2019) Copyright 2019 American Chemical Society. (d) Schematic of the integrated ethanol and acetone gas sensor by inkjet printing SnO_2 on interdigitated electrodes. The insert showed the sensor sensitivities under the exposure of ethanol and acetone.[143] Reproduced with permission from Lin *et al.*, Adv. Mater. **31**, 1804285 (2019). Copyright 2019 Wiley-VCH. (e) Optical graph and measurement of the inkjet-printed epidermal temperature sensor based on the graphene/PEDOT:PSS composite.[145]

modulate the channel current, which could be interpreted as the result of protonic doping or effective gate voltage shift. Elkington *et al.* inkjet-printed GO_x on the ion exchange membrane Nafion as the top gate electrode for glucose-sensitive thin-film transistor (OTFT).[131] They investigated the modification of the biosensor in terms of inkjet-printed film structures to reduce the response time and eliminate the device-to-device variation by avoiding aggregation problems in the drop-casting enzyme mixture. The OTFT-based biosensor achieved a linear response for glucose concentrations between 100 μM and 100 mM. To further demonstrate the practical wearable potentials, an inkjet-printed strain-accommodating organic electrochemical transistor was proposed by Li *et al.* [Fig. 4(b)].[132] The excellent stretchability and stable performance were attributed to the wavy surface structures of the PDMS substrate with the inkjet-printed conductive PEDOT:PSS layer, which interconnected the deformed electrodes and reduced the cracks. By inkjet printing Pt flakes and GO_x ink on the gold gate electrode for functionalization, the as-fabricated device achieved a reasonably low detection limit down to 1 μm and operated stably under 30% of omnidirectional strain and 15 mm of bending radius.

2. Pressure and strain sensors

The perception of mechanical stimuli, pressure, and strain is of great significance in acquiring tactile information and human physiological signals for wearable electronic sensors. Featuring conformal contact and lightweight attachment, the development of wearable sensors provides opportunities in high-sensitivity and prolonged real-time sensory applications. Examples include wearable pressure sensors and wearable strain sensors, which are developed for monitoring the arterial pulse and detecting subtle human motions, respectively.[59,133,134] The signal transduction process generally relies on the piezoresistive or capacitive mechanism that transforms mechanical stimuli into electrical responses. The production processes of the mentioned two types of sensors, which will be discussed in detail later, both involve depositing patterned conductive thin films on substrates, especially flexible ones for wearable applications. Compared with the conventional solution process such as transferring, spray coating, and screen printing, the inkjet printing techniques excel in cost-efficiency, patterning scale, and mask-free simple processing with high resolution for pressure and strain sensitive materials and devices.

Inkjet-printed piezoresistive sensors are based on the printed conductors whose resistance changes along with the applied pressure and strain. Casiraghi *et al.* proposed an inkjet-printed graphene strain sensor on paper with a high gauge factor of 125.[135] Water-based biocompatible graphene ink was printed between two contact pads and formed a 10 × 0.5 mm^2 sensitive line. High sensitivity was achieved by the reduced drop spacing and the increased printing layers that contributed to the underlying piezoresistivity because more deformation and microcracks upon strain can be induced in the thicker films. Lo *et al.* fabricated a wearable pressure sensor based on the inkjet-printed sensitive silver nanoparticle-based (AgNP) conductive layer.[136] The device was composed of a PDMS substrate, a serpentine-shaped AgNP active layer, and an encapsulation layer of acrylic foam tape. When the pressure was applied, the conductance of the active layer decreased due to the generation of microcracks. With the modification of stiffness and thickness to the polymeric substrate, the sensitivity of up to 0.48 kPa^{-1} can be achieved with a device demonstration of wearable sound wave detection and arterial pulse monitoring. In addition to paper and polymer substrates, conductive inks can also be inkjet-printed on hydrogels and transferred to arbitrary surfaces. Kang *et al.* utilized the physically cross-linked agarose and chemically cross-linked polyacrylamide (PAAm) as the hydrogel template that enabled contact or molding transfer for inkjet-printed SWCNTs [Fig. 4(c)].[137] The proposed hydrogel template could not only facilely transfer patterned nanonetworks of SWCNTs but also spontaneously separate conductive nanomaterials from the surfactant in the ink. With the help of non-adhesive, nanoporous structured, and moldable characteristics of the hydrogel, the inkjet-printed microstructured SWCNTs were perfectly transferred onto the PDMS substrates and functionalized as piezoresistive strain and pressure sensors for monitoring finger motions and arterial pulses. Apart from transferring templates, the hydrogel conductive inks may also participate in additional functionalities such as self-healable pressure sensing by a self-healing and strain-responsive injectable hydrogel-based ink.[138]

Capacitive sensing, which is another widely adopted method for mechanical sensing, works by measuring the capacitance variation in response to the external environment. There are mainly two types of capacitive sensor structures regarding the capacitance change mechanism. The first structure is based on the parallel-plate model where an insulating layer is sandwiched between two conductive electrodes. The capacitance of the device is changed with the deformation of the dielectric layer by applied pressure. Fu *et al.* inkjet-printed AgNP suspension on a PEN substrate as the bottom electrode and a paper substrate as the top electrode for integrating a parallel-plate capacitive sensor. Ecoflex, a commercial viscous silicone rubber, was adhered to the two electrodes as the dielectric layer and was also used to encapsulate the assembled capacitive sensor.[139] The presented durable and sensitive mechanical sensor could operate in piezoresistive or capacitive mode. The capacitance between the top and bottom electrodes was strongly related to the pressure applied, while the resistance of the bottom electrode could be measured simultaneously to determine the strain exerted on the device. Negligible interference was shown in the bimodal pressure and strain sensors, enabling inkjet-printed array implementation of the proposed sensors for mapping of the pressure and strain distribution. The second structure relies on the detection of mutual capacitance. When a capacitively grounded object approaches or touches the electrodes, the device capacitor will be disturbed by the edge electric field, which changes the capacitance. Ma *et al.* fabricated transparent touch sensor flexible PET substrates based on inkjet-printed PEDOT:PSS electrodes.[140] The top and bottom electrodes were printed in distinct patterns separately along with perpendicular directions. Dielectric PDMS was inkjet-printed at the intersection points of the electrodes and then thermally cured. The device enabled single and multiple touch detection with high sensitivity and demonstrated high flexibility with robustness for practical wearable use. Gilshtein *et al.* proposed an inorganic transparent conducting ITO film by inkjet printing with the organic coloring dye coating to increase the light absorption and enable efficient transient heating.[141] A flash lamp annealing technique was used to selectively and rapidly sinter the inkjet-printed ITO film for transparent capacitive touch sensors. As-prepared ITO-based electrodes can be inkjet-printed in trackpad network and square patterns for reliable detection of capacitance changes to accomplish wearable positioning and security tasks. Liu *et al.* further presented the inkjet-printed conductive silver microwire array (SMWA), which has a high pattern resolution (minimum single line width of 4.7 μm and controllable line-to-line spacing from 77 μm to 380 μm).[142] The SMWA structures were created by inkjet printing of the polydopamine (PDA) nanoparticle array based on the coffee-ring effect and used as the template for subsequent silver electroless plating. The as-fabricated continuous conductive SMWA was demonstrated as a flexible capacitive touch sensor with the orthogonally placed top and bottom electrodes that were separated by a dielectric tape. Detection of 20%–30% capacitance change by finger touching was realized with high durability under the cyclic bending test, indicating the potential for low-cost and facile fabrication of miniaturized wearable sensors.

3. Gas, temperature, and humidity sensors

Besides the aforementioned wearable sensors for the detection of human physiological signals, measurement of the external environment is also of great importance in wearable devices. Some parameters, such as gas, temperature, and humidity, are widely calculated to synthetically evaluate the atmosphere.

Integrating gas sensing functionality enables the warning of noxious gases and the detection of volatile biomarkers. Developing printable gas-sensitive components is beneficial for miniaturized wearable gas sensors that have the desired surface morphology for the facile integration process on flexible substrates. Inkjet-printed gas sensors are generally based on two sensing mechanisms, that is, chemiresistor and colorimetry. The chemiresistive approach relies on changes in the conductance of semiconducting inks in response to the exposure of target gases. Lin *et al.* fabricated a wearable room-temperature sensor for ethanol and acetone gas based on inkjet-printed SnO_2 with interdigitated silver interconnect [Fig. 4(d)].[143] The SnO_2 NP layer with a high surface-to-volume ratio showed good uniformity and favorable surface facets for gas absorption. When the sensor is in the environment containing reduction gas such as ethanol and acetone, free electrons would be released due to the reaction of gas with the adsorbed oxygen species on the SnO_2 surface, and thus, the material resistance would decrease. Moreover, the colorimetric gas sensors implement the detection of various gases in a visualized manner. Inkjet printing techniques enable the formation of different organics as an indicator array on a flexible substrate. Park *et al.* developed a volatile organic compound sensor by inkjet printing four different PDAs on the paper substrate.[144] The circular patterns with 0.4 cm diameter were printed with the diacetylene monomer ink and photopolymerized under ultraviolet irradiation. When exposed to unknown gases, the four PDA spots can represent a specific colorimetric response to the distinct functional groups and alkyl chain length. The color patterns were analyzed by a smartphone that compared the information with the database to determine the species of volatile organics.

Flexible and wearable electronics with temperature monitoring and disposable characteristics are applicable for wearable use. Vuorinen *et al.* leveraged the temperature-dependent resistance of PEDOT:PSS to implement a wave-patterned temperature sensor on the skin-conformable polyurethane substrate by inkjet printing [Fig. 4(e)].[145] The temperature response behavior was contributed to the core–shell microstructure of PEDOT:PSS where the outer PSS boundaries dominated the overall resistivity. When the temperature increased, the number of particle boundaries got smaller and the electrons easily passed through by gaining higher thermal energy, which caused the reduction in resistivity. The demonstrated device showed a sensitivity of 0.06%/°C and was fabricated by a scalable and cost-efficient manufacturing process. The humidity is another important environmental parameter that is generally based on resistive and capacitive responses. He *et al.* introduced an inkjet-printed wearable humidity sensor based on capacitance changes in GO and black phosphorus (BP).[146] Water-dispersed GO ink inkjet-printed on AgNP-based interdigitated electrodes was prepared from oxidation and exfoliation of graphite powder. The presence of oxygenated functional groups in the inks promoted the adsorption of water in the moist environment and caused an increase in the dielectric constant of the GO/BP films with strengthened polarization. The inkjet-printed device demonstrated a high capacitance sensitivity of over 11 in response to the 97% relative humidity with a fast response/recovery within 5 s, which showed the capability of detecting humidity variation with the simple fingertip approaching.

B. Flexible and wearable OLEDs

The organic light-emitting diodes (OLEDs), which use organic compounds to emit lights and display images in response to electric currents, are quite compatible with solution-based inkjet printing. The digital displays based on OLEDs are also suitable for flexible and wearable display applications because they have competitively low cost, wide vision field, fast response time, and high power efficiency within all the display techniques.[147,148] In recent years, inkjet printing of OLEDs has been widely investigated for practical processing on flexible substrates, especially the organic layers and electroluminescent materials. Hexagonal pixel-arranged real red–green–blue (RGB) active-matrix OLED (AMOLED) array panel was fabricated by Huo *et al.* with inkjet printing to achieve a high resolution of 403 ppi.[149] The prototype of inkjet-printed 55-in. and 8k-resolution AMOLED TV with 120 Hz also convinced that the inkjet printing process is promising and advantageous in the practical manufacturing of AMOLED displays with large dimension, high resolution, and low cost.[150]

Quantum dot light-emitting diodes (QLEDs) have been foreseen as the next-generation displays owing to the tunable size-related wavelength, narrow emission spectra, superior flexibility, and high stability. The quantum dots (QDs) composed of inorganic semiconductors are more stable, brighter, and lower-cost than the organic semiconductors, showing tremendous wearable-application potentials. The inkjet printing of high-resolution, uniform, and stable light-emitting QD pixel arrays with pixels of 500 per in. (500 ppi) was demonstrated by Kraus' group. As-prepared QLED arrays had the state-of-the-art quality for potential applications in standardized 8k commercial displays. Octane and cyclohexylbenzene (CHB) inks, which can be used to improve the attainable pixel quality, were inkjet-printed to form a stable 2 pL QLED dot with a diameter of 20 μm [Fig. 5(a)].[151] Li *et al.* demonstrated the fabrication of the QLED array oxide TFT backplane by inkjet-printing for the first time. The coffee-line patterns showed highly controllable and uniform morphology without nanopores in oxide dielectric layers. With the TFT array integration, active-matrix QLEDs were capable of displaying a red demo image, where one QLED pixel was equipped with two TFTs (the switching TFT and the driving TFT) and one capacitor.[152] High PL quantum yield (50%) PbS–CdS QDs with core–shell structures were demonstrated to fabricate high-quality QLED arrays via inkjet printing. With the assistance of solvent engineering and substrate patterning, as-prepared QLED devices showed a high external quantum efficiency of >2%, which was comparable to that made by the spin-coating process.[153] An impressive bilayer red QLED with a state-of-the-art external quantum efficiency of 11.6% in air was fabricated by Xie *et al.* [Fig. 5(b)].[154] They claimed the first report of inkjet-printed CBP-V and QD-based multilayer QLEDs that have longer lifetime, higher efficiency, and higher stability comparable to those by spin coating. Kim *et al.* demonstrated a skin-attachable QLED display device with an ultrathin thickness of only 5.5 μm that could be conformably integrated with the skin to reduce deformation failures. As-prepared ultrathin QLED displays successfully visualized designable information with good waterproof property, high brightness, and low operation voltages, which made it advantageous for wearable sensing (e.g., touch sensors and temperature sensors) in next-generation smart electronics. The ultrathin QLED display integrated with flexible circuits and wearable sensors

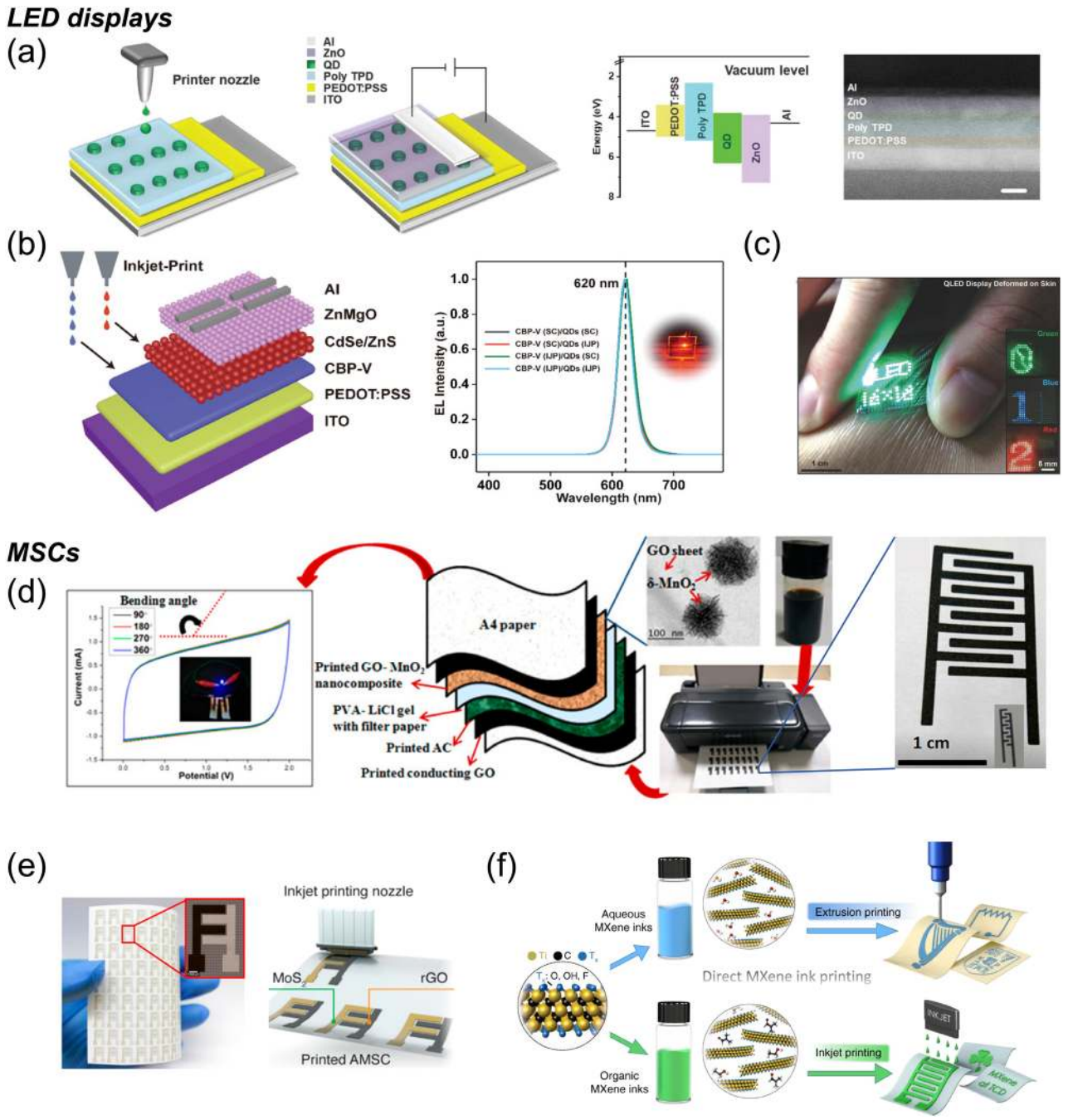

FIG. 5. (a) Left: schematic of inkjet-printed QLED pixels and the fully stacked device. Right: energy level diagram and cross-sectional micrograph of the stack (scale bar: 100 nm).[151] Reproduced with permission from Yang *et al.*, Adv. Opt. Mater. **8**, 1901429 (2019). Copyright 2019 Wiley-VCH. (b) Diagram of bilayer inkjet-printed QLEDs and the EL intensity of CBP-V-based red QLEDs.[154] Reproduced with permission from Xie *et al.*, Small **15**, 1900111 (2019). Copyright 2019 Wiley-VCH. (c) Photograph of the wearable display film on the skin.[155] Reproduced with permission from Kim *et al.*, Adv. Mater. **29**, 1700217 (2017). Copyright 2017 Wiley-VCH. (d) Schematic of inkjet-printed MnO_2/GO-based flexible supercapacitors on A4 paper substrates using an EPSON L130 printer. Left: CV curves of the flexible supercapacitors under various bending angles.[171] Reproduced with permission from P. Sundriyal and S. Bhattacharya, ACS Appl. Mater. Interfaces **9**, 38507 (2017) Copyright 2017 American Chemical Society. (e) Photograph and schematic of inkjet-printed arrays of 96 asymmetric MSCs on 10 × 10 cm^2 flexible EPSON photopaper.[172] Reproduced with permission from Shao *et al.*, ACS Nano **14**, 7308 (2020). Copyright 2020 American Chemical Society. (f) Schematic illustration of inkjet/extrusion printing of all-Mxene-printed ($Ti_3C_2T_x$) MSCs.[173] Reproduced with permission from Zhang *et al.*, Nat. Commun. **10**, 1795 (2019). Copyright 2019 Author(s), licensed under a Creative Commons Attribution 4.0 License.

yielded fully integrated sensor-display systems that can directly show sensing data of the human skin [Fig. 5(c)].[155]

C. Flexible and wearable TFTs

The flexible and stretchable thin-film transistors (TFTs) are basic building elements for electronic circuits, LED displays, sensors, data storage transistors, and power transmission devices. Flexible and wearable electronics are essentially integrated with TFTs as active matrices for backplanes and/or logic circuits to switch on/off and receive signals from the individual part.[156,157] These applications require inkjet-printed transistors with superior mechanical flexibility, sustainable electrical performance, and efficient printable processes that can be performed on a wide variety of substrates. The TFTs are divided into metal oxide TFTs and OTFTs that include organic field-effect transistors (OFETs). For most of the oxide TFTs, active materials such as the amorphous In–Ga–Zn–O (a-IGZO), Zn–Sn–O (ZTO), In–Zn–Sn–O (IZTO), and indium oxide (In_2O_3) are commonly inkjet-printed on flexible plastic substrates with SiO_2 and Al_2O_3 as the buffer layer. High field-effect mobility can be achieved by oxidizing the TFTs, but the metal-oxide materials have intrinsic poor mechanical properties in wearable applications.

For OTFTs of organic inks deposited on metal electrodes, the material interfaces normally show poor electrical contact with each layer on flexible substrates. This problem is caused by the mismatch between the metal electrode's high work function and the highest occupied molecular orbital of many *p*-type organic semiconductors. Mixing of organic electron acceptors into the silver inks was believed to efficiently improve the contact between electrodes and semiconductors and yielded tenfold improvement in FET mobility based on TIPS-pentacene without any direct patterning.[158] Many methods were investigated for addressing the contact issues caused by the incorporation of inkjet printing with other deposition processes. Kim *et al.* reported large-area FET arrays fabricated by combining the chemical vapor deposition (CVD)-grown MoS_2 monolayer with the inkjet-printed (Ag source/drain) electrodes in an optimized printing process (without special surface treatments). The Y-function method was proposed to characterize the surface energy, the electrical stability, and the contact resistance between the inkjet-printed electrodes and the CVD-grown monolayer.[159] For the all-inkjet-printed FETs, printing source/drain electrodes on the dielectric layer is more preferred (which is called bottom-gate and bottom-contact architecture (BGBC) than that on the semiconductor layer that is sensitive and fragile in the printing process. Feng *et al.* reported the all-inkjet-printed flexible BGBC–OFETs with low-voltage (<3 V) operation in an ambient environment. By blending small-molecule pentacene into polystyrene as an organic semiconductor layer, the state density at the semiconductor/gate dielectric interface was sharply reduced, showing great potential in low-voltage wearable systems.[160] High-performance TFTs fabricated by an aqueous-inkjet process can simplify the manufacturing process at relatively low temperatures with reduced cost. However, the modulation of aqueous ink is challenging due to the low solubility of organics and carbon-based materials in the printing of semiconductor layers and electrodes. Subramanian *et al.* demonstrated an all-aqueous-printed TFT with aluminum-doped cadmium oxide inks based on pure water via inkjet printing with low-temperature processing (≤250 °C). As-fabricated InO_x based TFTs showed a subthreshold slope lower than 150 mV dec^{-1}, a μ_{lin} up to 19 $cm^2\ V^{-1}\ s^{-1}$, and an ideal contact resistance of no more than 160 Ω cm^{-1}.[161] Hersam's group developed a low-consumption inkjet printing of high-performance short channel (150 nm–250 nm) SWCNT FETs with only 0.5 pg material consumption in a single ink droplet of 10 pL.[162] Vertical OFETs (VOFETs) have recently been explored to shorten the channel length by utilizing the vertical thickness of the active layer, rather than the line width in the plane. Compared with conventional lateral-channel OFETs, vertical architectures of VOFETs break the accuracy limitation of the inkjet printer system and thus promote the output current density as well as the switching speed. Fang *et al.* fabricated VOFET arrays on a plastic substrate via inkjet printing for the first time, which greatly simplified the previous solution-based process.[163] The VOFET array-based flexible AMOLED backplane exhibited a high current density of >6 mA cm^{-2} and can sustain repeated bending for 1000 times, showing considerable potential in next-generation wearable displays and electronic systems.

D. Flexible and wearable energy storage devices

Flexible energy storage and conversion devices should be essentially integrated into the portable systems to supply power and drive the wearable electronic devices. Various types of energy storage devices were widely investigated for wearable use such as supercapacitors, lithium-ion batteries, lithium–sulfur batteries, and metal–air batteries.[164] Inkjet printing enables the accurate single-step processing of each part in the energy storage and conversion devices, namely, electrodes, electrolytes, current collectors, and encapsulation layers with high flexibility, which increases the fabrication efficiency as well as the device performance.[165,166]

Flexible micro-supercapacitors (MSCs) are most widely utilized for wearable energy storage because of their intrinsically high power density, long-term stability, bending tolerance, and charging security.[167–169] Carbon and carbon-derived materials with large specific surface areas were commonly used in inkjet-printed supercapacitor electrodes. Lee *et al.* demonstrated all-solid-state on-chip MSCs with EHJ-printed active carbon as electrodes, which realized ultrahigh areal number density.[44] Choi *et al.* reported using A4 paper as substrates for inkjet-printed all-solid-state flexible supercapacitors. The pre-printed SWCNT/active carbon electrodes were coated by post-printed Ag nanowires networks that endowed the supercapacitors with impressive flexibility and improved electrical conductivity.[170] In addition to carbon, capacitive materials such as metal oxides were also qualified for inkjet-printed supercapacitor electrodes due to their high-performance pseudocapacitive property. Similarly, on A4 paper substrates, Sundriyal *et al.* proposed the inkjet printing of MnO_2 and GO/active carbon nanocomposites as the positive electrode for flexible asymmetric supercapacitors with PVA-LiCl as the gel electrolyte. The MnO_2-rich nanocomposites endowed the paper-based MSCs with excellent electrochemical performance (capacitance of 1023 F g^{-1} at 4 mA cm^{-2} and energy density of 22 mW h cm^{-3} at the power density of 0.099 W cm^{-3}) and high wearable endurance (capacity retention of 98.4% after 1000 bending cycles and 96.5% with five folds) [Fig. 5(d)].[171] Shao *et al.* utilized the electrohydrodynamic-assisted 3D crumpled stable MoS_2 inks without additives for the

inkjet-printed electrodes that were filled with open space for ion transport. As-prepared wearable MSCs exhibited an impressive areal energy density of 3.85 μW h cm^{-2} at 1.75 V. Moreover, an array of 96 inkjet-printed asymmetric MSCs on 10 × 10 cm^2 flexible EPSON photopaper was demonstrated, showing great integration of this system [Fig. 5(e)].[172] Recently, all-MXene-printed MSCs were proposed by Zhang *et al.* for the first time, which depended on the inkjet/extrusion-printing processing of additive-free and binary-solvent-free $Ti_3C_2T_x$ MXene inks in aqueous/organic solvents. As-assembled MSCs with interconnected nanosheet networks showed high durability for wearable applications, and they would not be peeled off by scotch tape from the flexible AlO_x-coated PET substrates due to strong interfacial adhesion [Fig. 5(f)].[173] Giannakou *et al.* demonstrated the inkjet-printed MSCs with state-of-the-art areal and volumetric specific capacitances of up to 155 mF cm^{-2} and 705 F cm^{-3}, respectively, which were based on nanoparticle-based NiO as film electrodes.[174] For real on-skin energy storage, they fabricated the symmetrical spiral-shaped MSCs on water-soluble PVA substrates and combined the inkjet with water-transfer printing to transfer them directly on the human skin like a temporary tattoo sticker. This inkjet printing/water-transferring approach provided a compelling platform toward real epidermal MSCs, which could be not only used for conformal energy storage but also referred to other flexible and wearable electronic device manufacturing.[175]

E. Other flexible and wearable devices

Data storage memory is a necessary component for advanced flexible electronic systems. Many methods such as transfer printing, microcontact printing, and various solution processes were developed for fabricating memories with fast switching speed, high retention time, and low programming voltages in wearable applications.[176] Casula *et al.* used inkjet-printed organic/metal nanoparticle/organic hybrid as the resistive layer of high-performance organic memory on PET flexible substrates. Recently, power-efficient, high-performance Pt/HfO_2/Ag non-volatile resistive memories were fabricated via inkjet printing.[177] The high-*k* HfO_2 dielectric endowed the memory with low set voltages, high switch ratios, and low switching current (~1 μA). However, the resistive memories fabricated by inkjet printing are normally assisted with the processes of CVD, electroplating, and photolithography. For fully inkjet-printing of flexible memories, Huber *et al.* worked on the Ag/spin-on-glass/PEDOT:PSS flexible memory cells and developed the inkjet printing process without additional steps or sacrificial layers.[178] Moreover, Casiraghi's group developed water-based, highly concentrated, and biocompatible inks that can be applied for fabrication of a variety of two-dimensional crystal heterostructures. They succeeded in demonstrating an all-inkjet-printed programmable logic memory device that stored "*words*" with a horizontal stripe (word line) and vertical stripe (bit lines).[179] The water-soluble polyacrylic acid solution was also reported to fabricate microstructured surface patterns via inkjet printing on pre-cured viscoelastic PDMS substrates. This technique was capable of pre-patterning dots, lines, and squares on the homogeneous surface and potentially providing an all-inkjet-printing process for more complex patterns with high resolution in flexible and wearable electronics.[180]

V. CONCLUSION AND OUTLOOK

Inkjet printing, which directly deposits solution-processable materials onto the given location of the substrate, shows enormous potential in the fabrication of flexible and wearable electronic devices. The unique advantages of inkjet printing include (i) the programmable and changeable patterning without extra masks; (ii) high-resolution patterning without limitations of the optical focus depth; (iii) no requirements for planar, conductive, or smooth printing substrates; (iv) superior processibility of both organic and inorganic materials; (v) minimized contamination in the non-contact printing process; (vi) cost-effective deposition (low ink consumption) at ambient environment; (vii) high-throughput and low-temperature processing; and (viii) excellent compatibility with other printing methods and fabrication technology.

Strategies for inkjet-printing mechanically flexible/stretchable wearable electronics based on versatile substrates are fully detailed and compared in this work. Recently reported techniques that solved the problems such as low conductivity of printed polymer materials, high sintering temperature of metallic materials, and low ink solubility of carbon-based materials have been reasonably summarized. Given all the impressive work, inkjet printing has garnered increasing attention from researchers in developing all-inkjet-printed electronic devices and wearable applications. Significant progress has been made in flexible and wearable electronics, e.g., sensors for mechanical stimuli, bio-substance detection, environmental parameter measurement, display arrays of OLEDs and QLEDs, heterostructured TFTs, energy-storage MCSs, and data-storage memories. Sophisticated techniques that promote inkjet printing, such as EHJ printing, aerojet printing, double-shot inkjet printing, pre-patterning, and vertically stack printing, are also desired in the future.

We anticipate promising technology applied science and engineering as well as commercial prospects for the inkjet-printed flexible and wearable electronics in the near future. Despite the encouraging progress mentioned above, some challenges in this specific issue remain to be addressed along with an equal number of opportunities. Through chemical or physical manipulation, more intrinsically flexible and stretchable inks are expected to prevent the pattern's cracking and delamination on the polymer or paper-based substrates. Besides, human epidermal devices demand elaborated design for higher stretching strain (>100%) to match modules of the human skin and inkjet-printed devices, which could be involved with finite element computation and multi-physics simulations. Meanwhile, the universal access to solve the nozzle clogging should be further developed, in order to guarantee a stable printing process and long-standing time with all types of inks. Moreover, it is imperative to have an all-inkjet-printed technique for various device fabrication, as well as the integration of multiple functional components synergistically in a single wearable electronic device. Finally, large-scale inkjet-printed electronic arrays should be realized in wearable devices to meet the practical requirements of high-performance sensing, computing, processing, and displaying. It is convincing that the development of advanced inkjet printing technologies would greatly contribute to the future of flexible and wearable electronics.

ACKNOWLEDGMENTS

The authors acknowledge the support of the National Natural Science Foundation of China under Grant Nos. 61825403, 61921005, and 61674078; the National Key Research and Development program of China under Grant No. 2017YFA0206302; and the PAPD program.

DATA AVAILABILITY

Data sharing is not applicable to this article as no new data were created or analyzed in this study.

REFERENCES

[1] M. Stoppa and A. Chiolerio, Sensors **14**, 11957–11992 (2014).
[2] J. S. Heo, J. Eom, Y.-H. Kim, and S. K. Park, Small **14**, 1703034 (2018).
[3] C. Wang, K. Xia, H. Wang, X. Liang, Z. Yin, and Y. Zhang, Adv. Mater. **31**, 1801072 (2019).
[4] W. Gao, H. Ota, D. Kiriya, K. Takei, and A. Javey, Acc. Chem. Res. **52**, 523 (2019).
[5] J. Kim, M. Kim, M. S. Lee, K. Kim, S. Ji, Y. T. Kim, J. Park, K. Na, K. H. Bae, H. Kyun Kim, F. Bien, C. Young Lee, and J. U. Park, Nat. Commun. **8**, 14997 (2017).
[6] A. Miyamoto, S. Lee, N. F. Cooray, S. Lee, M. Mori, N. Matsuhisa, H. Jin, L. Yoda, T. Yokota, A. Itoh, M. Sekino, H. Kawasaki, T. Ebihara, M. Amagai, and T. Someya, Nat. Nanotechnol. **12**, 907 (2017).
[7] J. Kim, A. S. Campbell, B. E.-F. de Ávila, and J. Wang, Nat. Biotechnol. **37**, 389 (2019).
[8] D. Wang, Y. Zhang, X. Lu, Z. Ma, C. Xie, and Z. Zheng, Chem. Soc. Rev. **47**, 4611 (2018).
[9] Z. Wu, Y. Wang, X. Liu, C. Lv, Y. Li, D. Wei, and Z. Liu, Adv. Mater. **31**, 1800716 (2019).
[10] P. Li, Y. Zhang, and Z. Zheng, Adv. Mater. **31**, 1902987 (2019).
[11] Y. T. Kwon, Y. S. Kim, S. Kwon, M. Mahmood, H. R. Lim, S. W. Park, S. O. Kang, J. J. Choi, R. Herbert, Y. C. Jang, Y. H. Choa, and W. H. Yeo, Nat. Commun. **11**, 3450 (2020).
[12] K. Sim, Z. Rao, Z. Zou, F. Ershad, J. Lei, A. Thukral, J. Chen, Q.-A. Huang, J. Xiao, and C. Yu, Sci. Adv. **5**, eaav9653 (2019).
[13] M. Zhu, T. He, and C. Lee, Appl. Phys. Rev. **7**, 031305 (2020).
[14] M. Gao, L. Li, and Y. Song, J. Mater. Chem. C **5**, 2971 (2017).
[15] N. Zhao, M. Chiesa, H. Sirringhaus, Y. Li, Y. Wu, and B. Ong, J. Appl. Phys. **101**, 064513 (2007).
[16] N. Godard, S. Glinšek, A. Matavž, V. Bobnar, and E. Defay, Adv. Mater. Technol. **4**, 1800168 (2019).
[17] D. Jang, D. Kim, and J. Moon, Langmuir **25**, 2629 (2009).
[18] J. R. Castrejon-Pita, N. F. Morrison, O. G. Harlen, G. D. Martin, and I. M. Hutchings, Phys. Rev. E **83**, 036306 (2011).
[19] Y. Liu and B. Derby, Phys. Fluids **31**, 032004 (2019).
[20] P. Delrot, M. A. Modestino, F. Gallaire, D. Psaltis, and C. Moser, Phys. Rev. Appl. **6**, 024003 (2016).
[21] Y. Kim, X. Ren, J. W. Kim, and H. Noh, J. Micromech. Microeng. **24**, 115010 (2014).
[22] K. X. Steirer, J. J. Berry, M. O. Reese, M. F. A. M. van Hest, A. Miedaner, M. W. Liberatore, R. T. Collins, and D. S. Ginley, Thin Solid Films **517**, 2781 (2009).
[23] B. J. de Gans, P. C. Duineveld, and U. S. Schubert, Adv. Mater. **16**, 203 (2004).
[24] B. Derby, Annu. Rev. Mater. Res. **40**, 395 (2010).
[25] R. Rioboo, M. Marengo, and C. Tropea, Exp. Fluids **33**, 112 (2002).
[26] A. L. Yarin, Annu. Rev. Fluid Mech. **38**, 159 (2006).
[27] Y. Liu, F. Li, L. Qiu, K. Yang, Q. Li, X. Zheng, H. Hu, T. Guo, C. Wu, and T. W. Kim, ACS Nano **13**, 2042 (2019).
[28] J. Lessing, A. C. Glavan, S. B. Walker, C. Keplinger, J. A. Lewis, and G. M. Whitesides, Adv. Mater. **26**, 4677 (2014).
[29] M. Kuang, J. Wang, B. Bao, F. Li, L. Wang, L. Jiang, and Y. Song, Adv. Opt. Mater. **2**, 34 (2014).
[30] L. Wu, Z. Dong, M. Kuang, Y. Li, F. Li, L. Jiang, and Y. Song, Adv. Funct. Mater. **25**, 2237 (2015).
[31] X. Yu, R. Xing, Z. Peng, Y. Lin, Z. Du, J. Ding, L. Wang, and Y. Han, Chin. Chem. Lett. **30**, 135 (2019).
[32] Y. Li, Q. Yang, M. Li, and Y. Song, Sci. Rep. **6**, 24628 (2016).
[33] R. D. Deegan, O. Bakajin, T. F. Dupont, G. Huber, S. R. Nagel, and T. A. Witten, Nature **389**, 827 (1997).
[34] W. D. Ristenpart, P. G. Kim, C. Domingues, J. Wan, and H. A. Stone, Phys. Rev. Lett. **99**, 234502 (2007).
[35] G. Hu, T. Albrow-Owen, X. Jin, A. Ali, Y. Hu, R. C. T. Howe, K. Shehzad, Z. Yang, X. Zhu, R. I. Woodward, T. C. Wu, H. Jussila, J. B. Wu, P. Peng, P. H. Tan, Z. Sun, E. J. R. Kelleher, M. Zhang, Y. Xu, and T. Hasan, Nat. Commun. **8**, 278 (2017).
[36] T. P. Bigioni, X.-M. Lin, T. T. Nguyen, E. I. Corwin, T. A. Witten, and H. M. Jaeger, Nat. Mater. **5**, 265 (2006).
[37] K. N. Al-Milaji, R. R. Secondo, T. N. Ng, N. Kinsey, and H. Zhao, Adv. Mater. Interfaces **5**, 1701561 (2018).
[38] E. He, D. Guo, and Z. Li, Adv. Mater. Interfaces **6**, 1900446 (2019).
[39] L. Wu, Z. Dong, N. Li, F. Li, L. Jiang, and Y. Song, Small **11**, 4837 (2015).
[40] J.-U. Park, M. Hardy, S. J. Kang, K. Barton, K. Adair, D. K. Mukhopadhyay, C. Y. Lee, M. S. Strano, A. G. Alleyne, J. G. Georgiadis, P. M. Ferreira, and J. A. Rogers, Nat. Mater. **6**, 782 (2007).
[41] S. An, C. Stambaugh, G. Kim, M. Lee, Y. Kim, K. Lee, and W. Jhe, Nanoscale **4**, 6493 (2012).
[42] K. Kaisei, N. Satoh, K. Kobayashi, K. Matsushige, and H. Yamada, Nanotechnology **22**, 175301 (2011).
[43] M. S. Onses, C. Song, L. Williamson, E. Sutanto, P. M. Ferreira, A. G. Alleyne, P. F. Nealey, H. Ahn, and J. A. Rogers, Nat. Nanotechnol. **8**, 667 (2013).
[44] K.-H. Lee, S.-S. Lee, D. B. Ahn, J. Lee, D. Byun, and S.-Y. Lee, Sci. Adv. **6**, eaaz1692 (2020).
[45] B. W. An, K. Kim, H. Lee, S.-Y. Kim, Y. Shim, D.-Y. Lee, J. Y. Song, and J.-U. Park, Adv. Mater. **27**, 4322 (2015).
[46] P. Zhou, H. Yu, W. Zou, Z. Wang, and L. Liu, Adv. Mater. Interfaces **6**, 1900912 (2019).
[47] M. A. Nilsson and J. P. Rothstein, J. Colloid Interface Sci. **363**, 646 (2011).
[48] Z. Zhang, X. Zhang, Z. Xin, M. Deng, Y. Wen, and Y. Song, Adv. Mater. **25**, 6714 (2013).
[49] H.-W. Kang, S. J. Lee, I. K. Ko, C. Kengla, J. J. Yoo, and A. Atala, Nat. Biotechnol. **34**, 312 (2016).
[50] S. Yoon, S. Sohn, J. Kwon, J. A. Park, and S. Jung, Thin Solid Films **607**, 55 (2016).
[51] H. Minemawari, T. Yamada, H. Matsui, J. Y. Tsutsumi, S. Haas, R. Chiba, R. Kumai, and T. Hasegawa, Nature **475**, 364 (2011).
[52] H. Sirringhaus, T. Kawase, R. H. Friend, T. Shimoda, M. Inbasekaran, W. Wu, and E. P. Woo, Science **290**, 2123 (2000).
[53] D. Li, W. Y. Lai, Y. Z. Zhang, and W. Huang, Adv. Mater. **30**, 1704738 (2018).
[54] Y. Nobusa, Y. Yomogida, S. Matsuzaki, K. Yanagi, H. Kataura, and T. Takenobu, Appl. Phys. Lett. **99**, 183106 (2011).
[55] Y. Takagi, Y. Nobusa, S. Gocho, H. Kudou, K. Yanagi, H. Kataura, and T. Takenobu, Appl. Phys. Lett. **102**, 143107 (2013).
[56] H. Jiang and B. Kaminska, ACS Nano **12**, 3112 (2018).
[57] Y. Li, L. Lan, S. Sun, Z. Lin, P. Gao, W. Song, E. Song, P. Zhang, and J. Peng, ACS Appl. Mater. Interfaces **9**, 8194 (2017).
[58] A. Al-Halhouli, H. Qitouqa, A. Alashqar, and J. Abu-Khalaf, Sens. Rev. **38**, 438 (2018).
[59] W. Cheng, J. Wang, Z. Ma, K. Yan, Y. Wang, H. Wang, S. Li, Y. Li, L. Pan, and Y. Shi, IEEE Electron Device Lett. **39**, 288 (2018).
[60] W. He, C. Wang, H. Wang, M. Jian, W. Lu, X. Liang, X. Zhang, F. Yang, and Y. Zhang, Sci. Adv. **5**, eaax0649 (2019).
[61] M. M. Hamedi, A. Ainla, F. Güder, D. C. Christodouleas, M. T. Fernández-Abedul, and G. M. Whitesides, Adv. Mater. **28**, 5054 (2016).

[62]S. Khan, L. Lorenzelli, and R. S. Dahiya, IEEE Sens. J. **15**, 3164 (2015).
[63]Y. S. Rim, S.-H. Bae, H. Chen, N. De Marco, and Y. Yang, Adv. Mater. **28**, 4415 (2016).
[64]A. J. Bandodkar, R. Nuñez-Flores, W. Jia, and J. Wang, Adv. Mater. **27**, 3060 (2015).
[65]J. Lee, S. Chung, H. Song, S. Kim, and Y. Hong, J. Phys. D: Appl. Phys. **46**, 105305 (2013).
[66]T. Kim, H. Song, J. Ha, S. Kim, D. Kim, S. Chung, J. Lee, and Y. Hong, Appl. Phys. Lett. **104**, 113103 (2014).
[67]J. Jiang, B. Bao, M. Li, J. Sun, C. Zhang, Y. Li, F. Li, X. Yao, and Y. Song, Adv. Mater. **28**, 1420 (2016).
[68]Y. Wang, Y. Wang, J.-j. Chen, H. Guo, K. Liang, K. Marcus, Q.-l. Peng, J. Zhang, and Z.-s. Feng, Electrochim. Acta **218**, 24 (2016).
[69]Y.-I. Lee and Y.-H. Choa, J. Mater. Chem. **22**, 12517 (2012).
[70]Y. Qin, A. U. Alam, M. M. R. Howlader, N.-X. Hu, and M. J. Deen, Adv. Funct. Mater. **26**, 4923 (2016).
[71]T. Zhang, X. Wang, T. Li, Q. Guo, and J. Yang, J. Mater. Chem. C **2**, 286 (2014).
[72]C. E. Knapp, J.-B. Chemin, S. P. Douglas, D. A. Ondo, J. Guillot, P. Choquet, and N. D. Boscher, Adv. Mater. Technol. **3**, 1700326 (2018).
[73]Y. Wang, C. Yan, S. Y. Cheng, Z. Q. Xu, X. Sun, Y. H. Xu, J. J. Chen, Z. Jiang, K. Liang, and Z. S. Feng, Adv. Funct. Mater. **29**, 1902579 (2019).
[74]N. Karim, S. Afroj, A. Malandraki, S. Butterworth, C. Beach, M. Rigout, K. S. Novoselov, A. J. Casson, and S. G. Yeates, J. Mater. Chem. C **5**, 11640 (2017).
[75]T. Carey, S. Cacovich, G. Divitini, J. Ren, A. Mansouri, J. M. Kim, C. Wang, C. Ducati, R. Sordan, and F. Torrisi, Nat. Commun. **8**, 1202 (2017).
[76]H. Shahariar, I. Kim, H. Soewardiman, and J. S. Jur, ACS Appl. Mater. Interfaces **11**, 6208 (2019).
[77]I. Kim, H. Shahariar, W. F. Ingram, Y. Zhou, and J. S. Jur, Adv. Funct. Mater. **29**, 1807573 (2019).
[78]J. Xu, H.-C. Wu, C. Zhu, A. Ehrlich, L. Shaw, M. Nikolka, S. Wang, F. Molina-Lopez, X. Gu, S. Luo, D. Zhou, Y.-H. Kim, G.-J. N. Wang, K. Gu, V. R. Feig, S. Chen, Y. Kim, T. Katsumata, Y.-Q. Zheng, H. Yan, J. W. Chung, J. Lopez, B. Murmann, and Z. Bao, Nat. Mater. **18**, 594 (2019).
[79]J. Yang, Z. Zhao, S. Wang, Y. Guo, and Y. Liu, Chem **4**, 2748 (2018).
[80]A. J. Heeger, Chem. Soc. Rev. **39**, 2354 (2010).
[81]Q. Liu, S. E. Bottle, and P. Sonar, Adv. Mater. **32**, 1903882 (2020).
[82]S. G. Bucella, A. Luzio, E. Gann, L. Thomsen, C. R. McNeill, G. Pace, A. Perinot, Z. Chen, A. Facchetti, and M. Caironi, Nat. Commun. **6**, 8394 (2015).
[83]A. Perinot and M. Caironi, Adv. Sci. **6**, 1801566 (2019).
[84]L. Bu, M. Hu, W. Lu, Z. Wang, and G. Lu, Adv. Mater. **30**, 1704695 (2018).
[85]F. Zhao, Y. Shi, L. Pan, and G. Yu, Acc. Chem. Res. **50**, 1734 (2017).
[86]L. Pan, G. Yu, D. Zhai, H. R. Lee, W. Zhao, N. Liu, H. Wang, B. C. K. Tee, Y. Shi, Y. Cui, and Z. Bao, Proc. Natl. Acad. Sci. U. S. A. **109**, 9287 (2012).
[87]L. Li, Y. Wang, L. Pan, Y. Shi, W. Cheng, Y. Shi, and G. Yu, Nano Lett. **15**, 1146 (2015).
[88]D. Zhai, B. Liu, Y. Shi, L. Pan, Y. Wang, W. Li, R. Zhang, and G. Yu, ACS Nano **7**, 3540 (2013).
[89]Z. Ma, W. Shi, K. Yan, L. Pan, and G. Yu, Chem. Sci. **10**, 6232 (2019).
[90]Y. Wang, C. Zhu, R. Pfattner, H. Yan, L. Jin, S. Chen, F. Molina-Lopez, F. Lissel, J. Liu, N. I. Rabiah, Z. Chen, J. W. Chung, C. Linder, M. F. Toney, B. Murmann, and Z. Bao, Sci. Adv. **3**, e1602076 (2017).
[91]Y. Joo, V. Agarkar, S. H. Sung, B. M. Savoie, and B. W. Boudouris, Science **359**, 1391 (2018).
[92]H. Yano, K. Kudo, K. Marumo, and H. Okuzaki, Sci. Adv. **5**, eaav9492 (2019).
[93]A. Dadvand, J. Lu, C. Py, T.-Y. Chu, R. Movileanu, and Y. Tao, Org. Electron. **30**, 213 (2016).
[94]S. Yoon, J. A. Park, H.-R. Lee, W. H. Yoon, D. S. Hwang, and S. Jung, Adv. Healthcare Mater. **7**, 1800050 (2018).
[95]T. G. Kim, H. J. Park, K. Woo, S. Jeong, Y. Choi, and S. Y. Lee, ACS Appl. Mater. Interfaces **10**, 1059 (2018).
[96]M. Grouchko, A. Kamyshny, C. F. Mihailescu, D. F. Anghel, and S. Magdassi, ACS Nano **5**, 3354 (2011).
[97]M. Tavakoli, M. H. Malakooti, H. Paisana, Y. Ohm, D. Green Marques, P. Alhais Lopes, A. P. Piedade, A. T. de Almeida, and C. Majidi, Adv. Mater. **30**, 1801852 (2018).
[98]Z.-K. Kao, Y.-H. Hung, and Y.-C. Liao, J. Mater. Chem. **21**, 18799 (2011).
[99]T. J. Simmons, D. Hashim, R. Vajtai, and P. M. Ajayan, J. Am. Chem. Soc. **129**, 10088 (2007).
[100]A. D. Winter, C. Jaye, D. Fischer, M. Omastová, and E. M. Campo, APL Mater. **2**, 066105 (2014).
[101]Y. Lu, X. Zong, Y. Wang, W. Zhang, Q. Wu, M. Liang, and S. Xue, J. Mater. Chem. C **7**, 14306 (2019).
[102]J. Luceño Sánchez, R. Peña Capilla, and A. Díez-Pascual, Polymers **10**, 1169 (2018).
[103]E. B. Secor, T. Z. Gao, M. H. Dos Santos, S. G. Wallace, K. W. Putz, and M. C. Hersam, ACS Appl. Mater. Interfaces **9**, 29418 (2017).
[104]E. B. Secor, B. Y. Ahn, T. Z. Gao, J. A. Lewis, and M. C. Hersam, Adv. Mater. **27**, 6683 (2015).
[105]V. Georgakilas, A. Demeslis, E. Ntararas, A. Kouloumpis, K. Dimos, D. Gournis, M. Kocman, M. Otyepka, and R. Zbořil, Adv. Funct. Mater. **25**, 1481 (2015).
[106]G. Bepete, E. Anglaret, L. Ortolani, V. Morandi, K. Huang, A. Pénicaud, and C. Drummond, Nat. Chem. **9**, 347 (2017).
[107]Y. Sui, A. Hess-Dunning, P. Wei, E. Pentzer, R. M. Sankaran, and C. A. Zorman, Adv. Mater. Technol. **4**, 1900834 (2019).
[108]G. Hu, J. Kang, L. W. T. Ng, X. Zhu, R. C. T. Howe, C. G. Jones, M. C. Hersam, and T. Hasan, Chem. Soc. Rev. **47**, 3265 (2018).
[109]S. Chung, K. Cho, and T. Lee, Adv. Sci. **6**, 1801445 (2019).
[110]F. Withers, H. Yang, L. Britnell, A. P. Rooney, E. Lewis, A. Felten, C. R. Woods, V. Sanchez Romaguera, T. Georgiou, A. Eckmann, Y. J. Kim, S. G. Yeates, S. J. Haigh, A. K. Geim, K. S. Novoselov, and C. Casiraghi, Nano Lett. **14**, 3987 (2014).
[111]M. Min, R. F. Hossain, N. Adhikari, and A. B. Kaul, ACS Appl. Mater. Interfaces **12**, 10809 (2020).
[112]K.-G. Zhou, N.-N. Mao, H.-X. Wang, Y. Peng, and H.-L. Zhang, Angew. Chem. **123**, 11031 (2011).
[113]A. G. Kelly, T. Hallam, C. Backes, A. Harvey, A. S. Esmaeily, I. Godwin, J. Coelho, V. Nicolosi, J. Lauth, A. Kulkarni, S. Kinge, L. D. A. Siebbeles, G. S. Duesberg, and J. N. Coleman, Science **356**, 69 (2017).
[114]J.-W. T. Seo, J. Zhu, V. K. Sangwan, E. B. Secor, S. G. Wallace, and M. C. Hersam, ACS Appl. Mater. Interfaces **11**, 5675 (2019).
[115]M. Vural, A. Pena-Francesch, J. Bars-Pomes, H. Jung, H. Gudapati, C. B. Hatter, B. D. Allen, B. Anasori, I. T. Ozbolat, Y. Gogotsi, and M. C. Demirel, Adv. Funct. Mater. **28**, 1801972 (2018).
[116]M. Bissannagari, T.-H. Kim, J.-G. Yook, and J. Kim, Nano Energy **62**, 645 (2019).
[117]M. Neophytou, F. Hermerschmidt, A. Savva, E. Georgiou, and S. A. Choulis, Appl. Phys. Lett. **101**, 193302 (2012).
[118]L. Qin, Q. Tao, X. Liu, M. Fahlman, J. Halim, P. O. Å. Persson, J. Rosen, and F. Zhang, Nano Energy **60**, 734 (2019).
[119]M. Mikolajek, T. Reinheimer, M. Muth, P. Hohwieler, M. J. Hoffmann, and J. R. Binder, Adv. Healthcare Mater. **20**, 1800318 (2018).
[120]T. Reinheimer, R. Azmi, and J. R. Binder, ACS Appl. Mater. Interfaces **12**, 2974 (2020).
[121]B. Reiser, L. González-García, I. Kanelidis, J. H. M. Maurer, and T. Kraus, Chem. Sci. **7**, 4190 (2016).
[122]D. J. Kang, Y. Jüttke, L. González-García, A. Escudero, M. Haft, and T. Kraus, Small **16**, 2000928 (2020).
[123]J. Lim, H. Jung, C. Baek, G.-T. Hwang, J. Ryu, D. Yoon, J. Yoo, K.-I. Park, and J. H. Kim, Nano Energy **41**, 337 (2017).
[124]Y. Liu, M. Pharr, and G. A. Salvatore, ACS Nano **11**, 9614 (2017).
[125]Z. Ma, S. Li, H. Wang, W. Cheng, Y. Li, L. Pan, and Y. Shi, J. Mater. Chem. B **7**, 173 (2019).
[126]Y. Yang and W. Gao, Chem. Soc. Rev. **48**, 1465 (2019).
[127]L. Li, L. Pan, Z. Ma, K. Yan, W. Cheng, Y. Shi, and G. Yu, Nano Lett. **18**, 3322 (2018).
[128]Z. Pu, J. Tu, R. Han, X. Zhang, J. Wu, C. Fang, H. Wu, X. Zhang, H. Yu, and D. Li, Lab Chip **18**, 3570 (2018).

[129]S.-W. Lee, K.-Y. Lee, Y.-W. Song, W. K. Choi, J. Chang, and H. Yi, Adv. Mater. **28**, 1577 (2016).
[130]T.-H. Kang, S.-W. Lee, K. Hwang, W. Shim, K.-Y. Lee, J.-A. Lim, W.-R. Yu, I.-S. Choi, and H. Yi, ACS Appl. Mater. Interfaces **12**, 24231 (2020).
[131]D. Elkington, M. Wasson, W. Belcher, P. C. Dastoor, and X. Zhou, Appl. Phys. Lett. **106**, 263301 (2015).
[132]Y. Li, N. Wang, A. Yang, H. Ling, and F. Yan, Adv. Electron. Mater. **5**, 1900566 (2019).
[133]S. Gong, W. Schwalb, Y. Wang, Y. Chen, Y. Tang, J. Si, B. Shirinzadeh, and W. Cheng, Nat. Commun. **5**, 3132 (2014).
[134]Z. Yang, Y. Pang, X.-l. Han, Y. Yang, J. Ling, M. Jian, Y. Zhang, Y. Yang, and T.-L. Ren, ACS Nano **12**, 9134 (2018).
[135]C. Casiraghi, M. Macucci, K. Parvez, R. Worsley, Y. Shin, F. Bronte, C. Borri, M. Paggi, and G. Fiori, Carbon **129**, 462 (2018).
[136]L. W. Lo, H. Shi, H. Wan, Z. Xu, X. Tan, and C. Wang, Adv. Mater. Technol. **5**, 1900717 (2019).
[137]T.-H. Kang, H. Chang, D. Choi, S. Kim, J. Moon, J. A. Lim, K.-Y. Lee, and H. Yi, Nano Lett. **19**, 3684 (2019).
[138]F. Ye, M. Li, D. Ke, L. Wang, and Y. Lu, Adv. Mater. Technol. **4**, 1900346 (2019).
[139]S. Fu, J. Tao, W. Wu, J. Sun, F. Li, J. Li, Z. Huo, Z. Xia, R. Bao, and C. Pan, Adv. Mater. Technol. **4**, 1800703 (2019).
[140]S. Ma, F. Ribeiro, K. Powell, J. Lutian, C. Møller, T. Large, and J. Holbery, ACS Appl. Mater. Interfaces **7**, 21628 (2015).
[141]E. Gilshtein, S. Bolat, G. T. Sevilla, A. Cabas-Vidani, F. Clemens, T. Graule, A. N. Tiwari, and Y. E. Romanyuk, Adv. Mater. Technol. **5**, 2000369 (2020).
[142]L. Liu, Y. Pei, S. Ma, X. Sun, and T. J. Singler, Adv. Healthcare Mater. **22**, 1901351 (2020).
[143]Y. Lin, J. Chen, M. M. Tavakoli, Y. Gao, Y. Zhu, D. Zhang, M. Kam, Z. He, and Z. Fan, Adv. Mater. **31**, 1804285 (2019).
[144]D.-H. Park, J.-M. Heo, W. Jeong, Y. H. Yoo, B. J. Park, and J.-M. Kim, ACS Appl. Mater. Interfaces **10**, 5014 (2018).
[145]T. Vuorinen, J. Niittynen, T. Kankkunen, T. M. Kraft, and M. Mantysalo, Sci. Rep. **6**, 35289 (2016).
[146]P. He, J. R. Brent, H. Ding, J. Yang, D. J. Lewis, P. O'Brien, and B. Derby, Nanoscale **10**, 5599 (2018).
[147]M. Choi, S.-R. Bae, L. Hu, A. T. Hoang, S. Y. Kim, and J.-H. Ahn, Sci. Adv. **6**, eabb5898 (2020).
[148]Y. Chu, C. Qian, P. Chahal, and C. Cao, Adv. Sci. **6**, 1801653 (2019).
[149]S. T. Huo, L. Q. Shao, T. Dong, J. S. Liang, Z. T. Bi, M. He, Z. Li, Z. Gao, and J. Y. Song, J. Soc. Inf. Disp. **28**, 36 (2020).
[150]Z. Wu, L. Yan, Y. Li, X. Feng, H. Shih, T. Kim, Y. Peng, J. Yu, and X. Dong, J. Soc. Inf. Disp. **28**, 418–427 (2020).
[151]P. Yang, L. Zhang, D. J. Kang, R. Strahl, and T. Kraus, Adv. Opt. Mater. **8**, 1901429 (2019).
[152]Y. Li, P. He, S. Chen, L. Lan, X. Dai, and J. Peng, ACS Appl. Mater. Interfaces **11**, 28052 (2019).
[153]G. Azzellino, F. S. Freyria, M. Nasilowski, M. G. Bawendi, and V. Bulović, Adv. Mater. Technol. **4**, 1800727 (2019).
[154]L. Xie, X. Xiong, Q. Chang, X. Chen, C. Wei, X. Li, M. Zhang, W. Su, and Z. Cui, Small **15**, 1900111 (2019).
[155]J. Kim, H. J. Shim, J. Yang, M. K. Choi, D. C. Kim, J. Kim, T. Hyeon, and D.-H. Kim, Adv. Mater. **29**, 1700217 (2017).
[156]H. Zhu, E. S. Shin, A. Liu, D. Ji, Y. Xu, and Y. Y. Noh, Adv. Funct. Mater. **30**, 1904588 (2019).
[157]M. Mizukami, S.-I. Cho, K. Watanabe, M. Abiko, Y. Suzuri, S. Tokito, and J. Kido, IEEE Electron Device Lett. **39**, 39 (2018).
[158]G. L. Whiting and A. C. Arias, Appl. Phys. Lett. **95**, 253302 (2009).
[159]T.-Y. Kim, M. Amani, G. H. Ahn, Y. Song, A. Javey, S. Chung, and T. Lee, ACS Nano **10**, 2819 (2016).
[160]L. Feng, C. Jiang, H. Ma, X. Guo, and A. Nathan, Org. Electron. **38**, 186 (2016).
[161]W. J. Scheideler, R. Kumar, A. R. Zeumault, and V. Subramanian, Adv. Funct. Mater. **27**, 1606062 (2017).
[162]S. Jang, B. Kim, M. L. Geier, M. C. Hersam, and A. Dodabalapur, Small **11**, 5505 (2015).
[163]Y. Fang, X. Wu, S. Lan, J. Zhong, D. Sun, H. Chen, and T. Guo, ACS Appl. Mater. Interfaces **10**, 30587 (2018).
[164]A. M. Zamarayeva, A. E. Ostfeld, M. Wang, J. K. Duey, I. Deckman, B. P. Lechêne, G. Davies, D. A. Steingart, and A. C. Arias, Sci. Adv. **3**, e1602051 (2017).
[165]J. Kim, R. Kumar, A. J. Bandodkar, and J. Wang, Adv. Electron. Mater. **3**, 1600260 (2017).
[166]T.-T. Huang and W. Wu, J. Mater. Chem. A **7**, 23280 (2019).
[167]H. Li and J. Liang, Adv. Mater. **32**, 1805864 (2020).
[168]L. Li, E. B. Secor, K.-S. Chen, J. Zhu, X. Liu, T. Z. Gao, J.-W. T. Seo, Y. Zhao, and M. C. Hersam, Adv. Healthcare Mater. **6**, 1600909 (2016).
[169]K. Yan, X. Sun, S. Ying, W. Cheng, Y. Deng, Z. Ma, Y. Zhao, X. Wang, L. Pan, and Y. Shi, Sci. Rep. **10**, 6227 (2020).
[170]K.-H. Choi, J. Yoo, C. K. Lee, and S.-Y. Lee, Energy Environ. Sci. **9**, 2812 (2016).
[171]P. Sundriyal and S. Bhattacharya, ACS Appl. Mater. Interfaces **9**, 38507 (2017).
[172]Y. Shao, J.-H. Fu, Z. Cao, K. Song, R. Sun, Y. Wan, A. Shamim, L. Cavallo, Y. Han, R. B. Kaner, and V. C. Tung, ACS Nano **14**, 7308 (2020).
[173]C. J. Zhang, L. McKeon, M. P. Kremer, S. H. Park, O. Ronan, A. Seral-Ascaso, S. Barwich, C. O. Coileain, N. McEvoy, H. C. Nerl, B. Anasori, J. N. Coleman, Y. Gogotsi, and V. Nicolosi, Nat. Commun. **10**, 1795 (2019).
[174]P. Giannakou, M. G. Masteghin, R. C. T. Slade, S. J. Hinder, and M. Shkunov, J. Mater. Chem. A **7**, 21496 (2019).
[175]P. Giannakou, M. O. Tas, B. Le Borgne, and M. Shkunov, ACS Appl. Mater. Interfaces **12**, 8456 (2020).
[176]G. Casula, B. Tkacz-Szczesna, Y. Busby, K. Ranoszek-Soliwoda, E. Tomaszewska, G. Celichowski, J. Grobelny, J.-J. Pireaux, P. Cosseddu, and A. Bonfiglio, Adv. Mater. Technol. **2**, 1700058 (2017).
[177]G. Vescio, G. Martín, A. Crespo-Yepes, S. Claramunt, D. Alonso, J. López-Vidrier, S. Estradé, M. Porti, R. Rodríguez, F. Peiró, A. Cornet, A. Cirera, and M. Nafría, ACS Appl. Mater. Interfaces **11**, 23659 (2019).
[178]B. Huber, P. B. Popp, M. Kaiser, A. Ruediger, and C. Schindler, Appl. Phys. Lett. **110**, 143503 (2017).
[179]D. McManus, S. Vranic, F. Withers, V. Sanchez-Romaguera, M. Macucci, H. Yang, R. Sorrentino, K. Parvez, S.-K. Son, G. Iannaccone, K. Kostarelos, G. Fiori, and C. Casiraghi, Nat. Nanotechnol. **12**, 343 (2017).
[180]J. Sun, C. Yun, B. Cui, P. Li, G. Liu, X. Wang, and F. Chu, Polymers **10**, 1209 (2018).